

Manuscript Number: JAAP-D-14-00422

Title: Structural characterization of semicokes produced from the pyrolysis of petroleum pitches

Article Type: Research Paper

Keywords: Pyrolysis; Petroleum pitches; Semicoke; Turbostratic structure

Corresponding Author: Dr. Yuda Yürüm, Ph.D

Corresponding Author's Institution: Sabanci University

First Author: Firuze Okyay Öner, Ph.D.

Order of Authors: Firuze Okyay Öner, Ph.D.; Alp Yürüm, Ph.D.; Yuda Yürüm, Ph.D

**Abstract:** The present study focuses on the structural analysis of anisotropic semicokes of the pyrolysis of petroleum pitches obtained under various experimental conditions of temperature and time. The overall objective is to provide further detailed information of factors which influence formation of anisotropy or turbostratic structures in resultant semicokes. Experiments were carried out under an argon atmosphere at the temperature range of 500-1000°C for 30, 60 and 120 minutes in a tube furnace. FTIR, <sup>1</sup>H-NMR, and <sup>13</sup>C-NMR results showed that the aromatic structure of the semicokes was increasing with respect to increasing temperature as well as increasing time. Aromaticity of the semicokes was calculated as 0.54 and 0.64, for pitch A at 500°C after 120 minutes, and pitch B at 600°C after 120 minutes, respectively. The intensity ratio between Raman "D" and "G" peaks, ID/IG (commonly used to characterize disorder in graphene structures) was observed to increase approximately linearly from 0.65 to 0.92 when the pyrolysis temperature of Pitch A was increased from 500°C to 900°C. XRD patterns of the semicokes showed the formation of some crystalline material with time and temperature. The average number of layers, calculated by the Debye-Scherrer technique using the XRD patterns of the semicokes, was between 5 and 10. SEM images of the semicokes indicated the presence of turbostratic structures. All the results of characterizations were consistent and indicated the formation of highly amorphous hydrocarbon materials that contain turbostratic structures. Treatments at higher temperatures increased formations of aromatic structure with increased crystallinity. Temperature seemed to be the dominating parameter of the pyrolysis reactions. As the pyrolysis temperature was increased, aromatic structure formation was favored with increased crystallinity in the semicokes.

Suggested Reviewers: M. Granda Ph.D.  
Professor, Instituto Nacional del Carbón  
mgranda@incar.csic.es  
Expert in pyrolysis of carbon materials

Vaclav Slovak Ph.D.  
Professor, Přírodovědecká fakulta, Ostravská univerzita v Ostravě  
vaclav.slovak@osu.cz  
Expert in pyrolysis of carbon materials

Zhancheng Guo Ph.D.

Dr., State Key Laboratory of Multiphase Complex Systems, Chinese Academy of Sciences  
guozc@home.ipe.ac.cn  
Expert on structure of chars

August 6, 2014

Professor K.J. Voorhees  
Colorado School of Mines  
Golden, Colorado  
USA

Dear Professor Voorhees,

I am submitting the manuscript “Structural characterization of semicokes produced from the pyrolysis of petroleum pitches” by Firuze Okyay Öner, Alp Yürüm and Yuda Yürüm for publication in Journal of Analytical and Applied Pyrolysis. The subject matter is original and has not been published elsewhere. I hope you will find it of interest and accept it for publication in Journal of Analytical and Applied Pyrolysis.

Best regards,

Yuda Yürüm  
Professor

# Structural characterization of semicokes produced from the pyrolysis of petroleum pitches

Firuze Okyay Öner<sup>a</sup>, Alp Yürüm<sup>b</sup> and Yuda Yürüm<sup>a\*</sup>

<sup>a</sup>*Materials Science and Nano Engineering Program, Faculty of Engineering and Natural Sciences, Sabanci University, Istanbul 34956, Turkey*

<sup>b</sup>*Sabanci University Nanotechnology Research and Application Center, SUNUM, Istanbul 34956, Turkey*

\*Corresponding author: [yyurum@sabanciuniv.edu](mailto:yyurum@sabanciuniv.edu)

## ABSTRACT

The present study focuses on the structural analysis of anisotropic semicokes of the pyrolysis of petroleum pitches obtained under various experimental conditions of temperature and time. The overall objective is to provide further detailed information of factors which influence formation of anisotropy or turbostratic structures in resultant semicokes. Experiments were carried out under an argon atmosphere at the temperature range of 500-1000°C for 30, 60 and 120 minutes in a tube furnace. FTIR, <sup>1</sup>H-NMR, and <sup>13</sup>C-NMR results showed that the aromatic structure of the semicokes was increasing with respect to increasing temperature as well as increasing time. Aromaticity of the semicokes was calculated as 0.54 and 0.64, for pitch A at 500°C after 120 minutes, and pitch B at 600°C after 120 minutes, respectively. The intensity ratio between Raman “D” and “G” peaks,  $I_D/I_G$  (commonly used to characterize disorder in graphene structures) was observed to increase approximately linearly from 0.65 to 0.92 when the pyrolysis temperature of Pitch A was increased from 500°C to 900°C. XRD patterns of the semicokes showed the formation of some crystalline material with time and temperature. The average number of layers, calculated by the Debye-Scherrer technique using the XRD patterns of the semicokes, was between 5 and 10. SEM images of the semicokes indicated the presence of turbostratic structures. All the results of characterizations were consistent and indicated the formation of highly amorphous hydrocarbon materials that contain turbostratic structures. Treatments at higher temperatures increased formations of aromatic structure with increased crystallinity. Temperature seemed to be the dominating parameter of the pyrolysis reactions. As the pyrolysis temperature was increased, aromatic structure formation was favored with increased crystallinity in the semicokes.

**Keywords:** Pyrolysis; petroleum pitches; semicoke; turbostratic structure

## 1. Introduction

The main raw material of this work, pitch, is a black, sticky solid material with very high viscosity. International Union of Pure and Applied Chemistry (IUPAC) [1] defines pitch as a solid material at room temperature which is the residue obtained after pyrolysis of organic materials or distillation of tar. It is also indicated that pitch is a complex form consisting of aromatic hydrocarbons and heterocyclic compounds. The feedstock affects the aromatic to aliphatic hydrogen ratio of pitch that indicates the hydrogen aromaticity. This ratio is reported to be in between 0.3 and 0.9 [1].

Pitch can be obtained either from coal-tar or petroleum. Both pitch types are complex mixtures of organic molecules that mainly consist of polycyclic aromatic hydrocarbons (PAH). Coal-tar pitch includes more hetero-aromatic compounds in addition to PAHs, while petroleum pitch includes numerous alkyl-substituted PAHs [2]. This polycyclic aromatic structure of pitches results in isotropic or anisotropic semicoke formation with high yields during heat treatment processes. Due to this chemical property of pitches, main applications rely on their chemical characteristic structure.

Commercially, petroleum and coal-tar pitches turned from worthless wastes into important raw materials of aromatic and carbonaceous materials. Manufacturing of graphite electrodes (for aluminum and steel industry), PAHs (for lithium ion batteries and hydrogen storage), carbon fibers, carbon-carbon composites, nuclear graphites, activated carbons, mesophase carbon fibers, and mesocarbon microbeds can be obtained by pyrolysis and carbonization processes of pitches [3-5]. High yields of graphitic carbons and semicokes can be achieved during pitch pyrolysis reactions [2]. It is very difficult to explain the mechanism of pitch pyrolysis, because of the complex chemical structure of the material. There are thousands of different types of molecules with various molecular sizes and functions in pitch structure. For this reason, there is a potential for each different molecule to react distinctively. Just like the complex chemistry of pitches, a complex thermal chemistry occurs during pyrolysis of pitches.

In earlier surveys on the organic chemistry of carbons, XRD, FTIR, and  $^{13}\text{C}$  NMR have been generally used to characterize the functional groups and structural parameters in kerogen [6,7].  $^{13}\text{C}$  NMR spectroscopy has been utilized for coal research since the late 1970s [8-10]. Cao et al. worked on chemical structure changes in kerogen from bituminous coal and reviewed the characterization of kerogen using advanced  $^{13}\text{C}$  NMR spectroscopy [11,12].

1 FTIR spectroscopy was used to determine the absorptivity of aromatic and aliphatic C–H  
2 bonds [13], aromaticity, and to analyze the carboxyl groups [14]. The chemical structure of  
3 coals and carbons was studied by FTIR and Py-GC/MS. Reactive functional groups and  
4 aliphatic hydrocarbons released with increasing pyrolysis temperature [15] were determined  
5 by FTIR and GC/MS. In a new study, the structural characteristics of thermally  
6 metamorphosed coal were investigated using FTIR spectroscopy and XRD analysis [16].  
7 Recently, the structures of chars in inertinite-rich coal were characterized by X-ray  
8 diffraction.  
9

10  
11  
12  
13  
14 Our purpose in this research was to investigate structural evolution of the anisotropic  
15 semicokes by following the changes in their molecular, crystalline and morphological  
16 structures under different pyrolysis conditions. Variation of carbon structures during pyrolysis  
17 at different temperatures and durations were investigated by thermogravimetric analysis  
18 (TGA), scanning electron microscopy (SEM), <sup>13</sup>C NMR spectroscopy, Fourier Transform  
19 Infrared Spectroscopy (FTIR), Raman Spectroscopy (RAMAN), and powder X-ray diffraction  
20 (XRD).  
21  
22  
23  
24  
25  
26  
27

## 28 **2. Materials and method**

### 29 *2.1. Raw materials*

30  
31  
32  
33 The main raw materials of this study were two petroleum pitches obtained from  
34 Turkish Petroleum Refineries Company (TÜPRAŞ) and they were named as Pitch A and  
35 Pitch B. Elemental analyses (C, H, N, and S) of pitch A and pitch B were conducted at the  
36 Instrumental Analysis Laboratory of the TUBITAK Marmara Research Center, Gebze by  
37 using standard methods. The data of the elemental analyses of the pitch samples are presented  
38 in Table 1.  
39  
40  
41  
42  
43  
44

### 45 *2.2. Pyrolysis of petroleum pitches*

46  
47  
48 10-15 g of pitch samples placed in an alumina boat were pyrolyzed in a quartz tube  
49 furnace. The pyrolysis experiments were carried under an argon atmosphere with a flow rate  
50 of 2.5 L/min. In order to investigate the effect of pyrolysis temperature and duration on the  
51 formation of solid products, various temperature and time sets were performed during  
52 experimental studies. The pyrolysis experiments were conducted in the range of 500°C-  
53 1000°C with 100°C degrees of increment and the pyrolysis durations were 30, 60, and 120  
54 minutes. The tube furnace was heated to the temperature of the experiment with a heating rate  
55  
56  
57  
58  
59  
60

1 of 50°C/min. Gaseous products of pyrolysis accumulated in a gasometer and volatile products  
2 were collected in condensers. Semicokes which were the main interest of the present work,  
3 were cooled down to room temperature and further analyzed for characterization.  
4  
5

### 6 2.3. Characterization of the solid carbonaceous products 7

8  
9 FTIR spectra of the Pitch A and Pitch B, and semicokes obtained after pyrolysis  
10 experiments were examined by using a Bruker Equinox 55 FTIR spectrometer equipped with  
11 an ATR system by co-adding 20 scans over the range 600-4000 cm<sup>-1</sup> performed at 1 cm<sup>-1</sup> of  
12 digital resolution.  
13  
14

15  
16 <sup>1</sup>H-NMR spectra of the pitches were measured utilizing a Varian Unity Inova 500  
17 mHz NMR spectrophotometer and benzene-d<sub>6</sub> was used as a solvent. The molecular structure  
18 and aromaticity of the semicokes formed after pyrolysis experiments were investigated by  
19 solid-state <sup>13</sup>C-NMR spectroscopy techniques utilizing a Varian Unity Inova 500 mHz  
20 spectrophotometer with cross polarization (CP) and magic angle spinning (MAS).  
21  
22

23  
24 Structural changes in semicokes were also analyzed using a Renishaw Raman  
25 spectrometer equipped with a Via Reflex Raman Microscopy System (Renishaw Plc., New  
26 Mills, Wotton under-Edge Gloucestershire, UK) using a 514 nm argon ion laser in the range  
27 of 100 to 3200 cm<sup>-1</sup>.  
28  
29

30  
31 X-ray diffraction was used to determine the evolution in the crystal structure and  
32 number of graphene layers of the turbostratic semicokes. A Bruker AXS advance powder  
33 diffractometer fitted with a Siemens X-ray gun, using Cu K<sub>α</sub> radiation (λ= 1.5406Å) was  
34 used to measure the X-ray diffraction patterns. The solid samples were rotated at 10 rpm and  
35 swept from 2θ = 10° through to 90° using default parameters of the program of the  
36 diffractometer that was equipped with Bruker AXS Diffrac PLUS software. The X-ray  
37 generator was set to 40 kV at 40 mA. All the XRD measurements were repeated at least two  
38 times and the results were the average of these measurements.  
39  
40

41  
42 The XRD patterns were analyzed for the structural parameters by using the by using  
43 the classical Debye-Scherrer equations [17]:  
44  
45

$$46 t = 0.90\lambda / \beta_{002} \cos \theta_{002}$$

$$47 n = t / d_{002}$$

48  
49 where  $t$  represents the thickness,  $\beta$  the full width half maxima (FWHM),  $d_{002}$  the interlayer  
50 spacing, and  $n$  is the number of graphene sheets. FWHM values of the (002) peaks were  
51  
52  
53  
54  
55  
56  
57  
58  
59  
60  
61  
62  
63  
64  
65

1  
2  
3  
4  
5  
6  
7  
8  
9  
10  
11  
12  
13  
14  
15  
16  
17  
18  
19  
20  
21  
22  
23  
24  
25  
26  
27  
28  
29  
30  
31  
32  
33  
34  
35  
36  
37  
38  
39  
40  
41  
42  
43  
44  
45  
46  
47  
48  
49  
50  
51  
52  
53  
54  
55  
56  
57  
58  
59  
60  
61  
62  
63  
64  
65

calculated by the Bruker axs Diffrac PLUS software provided with the Bruker axs advance powder diffractometer.

The morphology of semicokes obtained from pitch pyrolysis was also investigated by scanning electron microscopy (SEM) analyses using a Leo Supra 35VP Field Emission scanning electron microscope.

### 3. Results and discussion

#### 3.1. Pyrolysis of pitches

At the pyrolysis temperatures the pitches disintegrated into gaseous and volatile liquid products leaving back relatively smaller amounts of solid products. The production of volatiles finished at about 550°C and the gas production finished around 600°C, for both of the pitches. The solid products that were obtained at these temperatures are called semisemicokes [18]. The process of conversion of a pitch material to the solid 'green' coke probably involved an intermediate phase, a liquid-crystal phase or mesophase. Semicoke is defined as a carbonaceous material intermediate between a fusible mesophase pitch and a non deformable green coke, produced by incomplete carbonization at temperatures between the onset of fusion of pitch ca 620 K (347°C) and complete devolatilization [1]. Therefore, semicoke still contains volatile matter.

Fig.s 1 a and 1 b present the yields of semicokes with respect to pyrolysis temperature and duration for Pitch A and Pitch B, respectively. The yields of semicokes for both of the pitches at all conditions changed between 4.0 and 15.0 percent. The yield of semicokes of both of Pitch A and Pitch B decreased as the duration of pyrolysis reaction increased. Yields of the semicokes obtained at 30 minutes and 60 minutes were higher compared to the yields at 120 minutes for both of the pitches. As the pyrolysis temperature was increased from 500°C to 1000°C, the yield of the semicokes decreased substantially. Degradation of macromolecular structures was favored at the higher temperatures of pyrolysis. Bond cleavage of the macromolecular structures in the pitch, occurring at temperatures close to 1000°C produced bigger amounts of gases and volatiles and thus less amount of semicokes.

### 3.2. Structural analyses

#### 3.2.1. FTIR spectroscopy

FTIR spectra of Pitch A and Pitch B, shown in Fig. 2 a and 2 b, respectively, demonstrated their complex structures. Most of these bands have contributions from both aromatic and aliphatic compounds and methyl derivatives. More specifically, the bands near 2850-2920  $\text{cm}^{-1}$  were due to  $\text{CH}_3$  and  $\text{CH}_2$  stretching of methyl or methylene groups, peaks in the range of 1550-1600  $\text{cm}^{-1}$  were because of aromatic compounds and those at 1400-1460  $\text{cm}^{-1}$  are characteristic bands for of aliphatic chains [19].

FTIR spectra also included a strong stretching of aliphatic groups attached to aromatic compounds at 2850-2900  $\text{cm}^{-1}$ , ring vibration of aromatic hydrocarbons at 1600  $\text{cm}^{-1}$ , a strong peak of aliphatic hydrocarbon chains at 1458  $\text{cm}^{-1}$ , and methylbenzene derivatives at 1375  $\text{cm}^{-1}$ , several distinct peaks of C-H bending and probably a sulfur stretching in the finger print region between 700 and 865  $\text{cm}^{-1}$ . More precisely, the bands at 2919 and 2850  $\text{cm}^{-1}$  represented symmetric stretching of saturated hydrocarbons of  $-\text{CH}$  and  $>\text{CH}_2$  respectively. While ring vibrations of aromatic compounds were observed at 1600  $\text{cm}^{-1}$ , the  $-\text{CH}_3$  asymmetric and symmetric bending of aliphatic hydrocarbon chains were at 1458  $\text{cm}^{-1}$  and 1375  $\text{cm}^{-1}$  respectively. Finally, C-H bending was located at 723, 809 and 863  $\text{cm}^{-1}$  [19]. The comparison of the spectra of Pitch A and Pitch B demonstrated that Pitch A probably had more aromatic structure due to the ratio of the aliphatic and aromatic peaks (in the range of 1400-1450  $\text{cm}^{-1}$  and 1550-1650  $\text{cm}^{-1}$ , respectively). FTIR spectrum of the Pitch B showed that the peaks of aliphatic compounds' intensities were stronger than the aromatic peaks relative to the aliphatic peaks of Pitch A.

The FTIR spectra of the semicokes obtained after the pyrolysis of Pitch A and Pitch B are presented in Fig. 3. The spectra of carbonaceous products obtained from Pitch A showed significant changes with respect to increasing pyrolysis temperature. The spectra of carbonaceous products clearly demonstrated a change in the chemistry of products as the pyrolysis temperature was increased. The significant decrease in the peaks and intensities of aliphatic groups at 2850-2920  $\text{cm}^{-1}$  and 1400-1450  $\text{cm}^{-1}$ , and increase in the ring vibrations of the aromatic hydrocarbons at 1550-1650  $\text{cm}^{-1}$  was an important result. The decrease in the aliphatic hydrocarbons with increasing pyrolysis temperature was an expected result, because higher pyrolysis temperatures favor formation of aromatic carbons [2]. The spectra of samples from the pyrolysis of Pitch B demonstrated that ratio of intensities of aliphatic groups (1380-

1450  $\text{cm}^{-1}$ ) to aromatic groups (1480-1650  $\text{cm}^{-1}$ ) decreased with increasing pyrolysis temperature. In addition, the bands of aliphatic groups attached to aromatic compounds (2850-2920  $\text{cm}^{-1}$ ) disappeared totally. These were the evidences that heat treatment at higher temperatures favored the formation of more aromatic structures in pitch pyrolysis, as well as degradation of aliphatic compounds.

In addition to temperature effect on molecular structure, pyrolysis duration also affected the structure of the pyrolysis products. The FTIR spectra of the semicokes obtained from the pyrolysis of Pitch A produced at 800°C after 30, 60, and 120 minutes are presented in Fig. 4. It was apparent that stretching of aliphatic groups attached to aromatic compounds at 2850-2920  $\text{cm}^{-1}$  was lost, and the range of ring vibrations of aromatic hydrocarbons increased from 1540-1575  $\text{cm}^{-1}$  to 1500-1660  $\text{cm}^{-1}$  with stronger intensities. Moreover the aliphatic hydrocarbon chains were lost (it was observed at the spectrum of 2 hour of pyrolysis with one peak which has a lower intensity than the aromatic hydrocarbons). The oxidation bands around 1700  $\text{cm}^{-1}$  occurred after 1 hour of heat treatment, and methyl rocking around 1120-1150  $\text{cm}^{-1}$  formed after 1 hour of treatment. As a result, aromatic structure formation was favored with increasing pyrolysis duration. In addition, the ratio of aliphatic intensities to aromatic intensities decreased continuously and the aliphatic groups attached to the aromatics were eliminated with increasing duration of heat treatment.

### 3.2.2. $^1\text{H}$ and $^{13}\text{C}$ NMR spectroscopy

The molecular structures of Pitch A and Pitch B were examined by  $^1\text{H}$ -NMR in addition to FTIR analyses. Fig. 5 represents the  $^1\text{H}$ -NMR spectra of Pitch A and Pitch B in the range of 0 to 7 ppm. Both spectra of Pitch A and Pitch B contained peaks of saturated hydrocarbons between 0.5-1.3 ppm. More specifically, there were peaks of primary hydrocarbons ( $\text{R-CH}_3$ ) at 0.9 ppm, secondary hydrocarbons ( $\text{R}_2\text{-CH}_2$ ) at 1.3 ppm, and probably cyclohydrocarbons around 0.5 ppm in the both spectra of Pitch A and Pitch B [20]. When the range between 4-7 ppm was magnified, inset Fig.s in Fig. 5, it was seen that pitches also contained aromatic structures.

The molecular structures of the semicokes were also analyzed by solid-state  $^{13}\text{C}$ -NMR. Fig. 6 and Fig. 7 represent the solid-state  $^{13}\text{C}$ -NMR spectra of semicokes after 2 hours of pyrolysis of Pitch A and Pitch B, respectively. Deconvolution of the  $^{13}\text{C}$  NMR spectra revealed detailed information about the functionalities present in the semicokes after the pyrolysis (Fig. 8). Fig. 8 a and 8 b presents the deconvoluted  $^{13}\text{C}$  NMR spectra of the

1  
2  
3  
4  
5  
6  
7  
8  
9  
10  
11  
12  
13  
14  
15  
16  
17  
18  
19  
20  
21  
22  
23  
24  
25  
26  
27  
28  
29  
30  
31  
32  
33  
34  
35  
36  
37  
38  
39  
40  
41  
42  
43  
44  
45  
46  
47  
48  
49  
50  
51  
52  
53  
54  
55  
56  
57  
58  
59  
60  
61  
62  
63  
64  
65

semicokes of Pitch A at 500°C after 120 minutes of pyrolysis and Pitch B at 600°C after 120 minutes of pyrolysis. Both of the spectra contained several deconvoluted peaks that were hidden under some of the peaks. The exact positions of all of the peaks in the spectra are shown in the spectra. Peaks located near 210-211 ppm are due to Ar-C=O, and peaks near 167-172 ppm are due to Ar-COOH. Ar-C peak is located at 137.5 ppm and near 124-125 ppm Ar-CH peak exists. Around 95 ppm Ar-CH exists and near 80-84 ppm peaks exist due to aliphatic CH-OH, CH<sub>2</sub>-OH and CH<sub>2</sub>-O-. Finally peaks near 38-39 ppm are due to methylene, CH<sub>2</sub>, and those near 21-17 ppm are due to methyl, CH<sub>3</sub> groups [21,22]. Percent areas of functional groups calculated from the deconvoluted <sup>13</sup>C NMR spectra of the carbonaceous solid residues obtained from Pitch A and Pitch B are presented in Table 2. Aromaticity of the carbonaceous semicokes was calculated as 0.54 and 0.64, for pitch A at 500°C after 120 minutes, and pitch B at 600°C after 120 minutes, respectively.

As the temperature increased, peaks of aliphatic compounds were lost before aromatic compounds. Until 900°C, the intensity of aromatic groups was higher than that of aliphatic groups, indicating that it was harder to degrade aromatic structures. The peak of carbonyl groups was lost after 800°C in the semicoke of Pitch B whereas it was lost at 700°C in the pyrolysis of Pitch A. In addition, the intensities of the peaks were lower in Pitch B pyrolysis products with respect to pyrolysis products of Pitch A. This result showed that there were some structural differences in the pitches studied and this affected the structure of pyrolysis products. Similar to Pitch A pyrolysis, intensities of all the peaks of the pyrolysis products of Pitch B decreased with increasing pyrolysis temperature. More specifically, the aliphatic peaks were lost before aromatic groups and at 1000°C there was a broad peak due to aromatic structures. These results supported the findings from the FTIR spectra that indicated the increase of aromaticity with increasing pyrolysis temperature. Using the procedure in reference [23], the aromaticity of semicokes from Pitch A increased from 0.54 to 0.81 as temperature was increased from 500 to 800°C. The aromaticity of Pitch B semicokes were 0.64 and 0.67 for 600°C and 800 °C, respectively. This proved that heat treatments at higher pyrolysis temperatures favored formation of aromatic structures, which was consistent with FTIR results. Pitch pyrolysis favored aromatic structure formation as indicated by their higher intensities, loss of aromatic peaks at longer durations of pyrolysis, as well as higher aromaticity ratios.

### 3.2.3. Raman spectroscopy (RAMAN)

Raman spectroscopy is a powerful method due to its sensitivity not only to the crystalline structure but also to the molecular structures of the compounds [24]. Nowadays, Raman spectroscopy is also used in the determination of the number of graphene layers [25]. Raman spectra of carbon materials usually divided in to two regions of first and second order. For perfect graphite, there is only one peak called the G band, which is at  $1580\text{ cm}^{-1}$ . The other important three peaks of graphite are the G' band (the overtone of the G line) around  $3248\text{ cm}^{-1}$ , the D band around  $1350\text{ cm}^{-1}$  and the D' band (the overtone of the D line) around  $2700\text{ cm}^{-1}$  [25]. The intensity ratio of the D band and G band is related to the degree of carbon structural order [24]. Therefore, the D band depends on the amount of the disorder of the graphitic materials. The G peak is due to the bond stretching of all pairs of  $\text{sp}^2$  atoms in both rings and chains. The D peak is due to the breathing modes of  $\text{sp}^2$  atoms in rings [26]. Raman spectra of carbon structures produced after 2 hours of pyrolysis of Pitch A after at 900, 700, and  $500^\circ\text{C}$  and after 2 hours of pyrolysis of pitch B at 1000, 700, and  $500^\circ\text{C}$  are presented in Fig.s 9 a and 9 b, respectively. In both spectra of Pitch A and Pitch B semicokes, significant D and G bands was observed.

The differences in the spectra clearly indicated that there was a change in the crystalline structure with respect to increasing pyrolysis temperature. The shifting of D band to higher wavenumbers is due to increasing incident laser excitation energies and the relative intensity of the D band depends on the amount of disorder [27]. So, the spectra in the Fig.s 9a and 9b indicates that as pyrolysis temperature was increased, the crystallite size was also increased. That was accompanied with a decrease in the disorder seen from the decreasing intensity of D band [27,28]. Since G band is due to bond stretching of  $\text{sp}^2$  atoms in both ring and chains, a decrease in the G band intensity is related to the decreasing of number of layers in graphitic structure [27]. For this reason, spectra indicated a decrease of graphene layers with increasing pyrolysis temperature. Additionally, the intensity ratio of D and G bands shows disorder of carbon structure [24]. As the pyrolysis temperature increased,  $I_D/I_G$  also increased from 0.65 to 0.79 and finally to 0.92 indicating that disorder in the structures of pyrolyzed Pitch A was decreasing with increasing pyrolysis temperature. Table 3 and 4 present the parameters of D and G bands, respectively.

In addition to the effect of pyrolysis temperature, the effect of pyrolysis duration on the formation of crystalline structures in pyrolysis of Pitch A at  $900^\circ\text{C}$  and  $500^\circ\text{C}$  were also

1 demonstrated in Fig.s 10 a and 10 b, respectively. For the higher pyrolysis temperature, the  
2 lowest D and G band intensities were obtained after 1 hour of pyrolysis and the highest  
3 intensities were obtained after 2 hours of pyrolysis. The  $I_D/I_G$  ratios were 0.95, 0.85, and 0.92  
4 as the pyrolysis durations were 30, 60, and 120 minutes, respectively. However, as illustrated  
5 in Fig. 10 b, at lower temperatures both intensities of the D and G bands decreased with  
6 decreasing duration. At lower temperatures, shorter residence time produced graphitic  
7 structures with less disorder. In addition,  $I_D/I_G$  ratios were 0.70, 0.64, and 0.65 for 30, 60, and  
8 120 minutes of pyrolysis respectively.

#### 15 3.2.4. Powder x-ray diffractometry (XRD)

18 Microcrystalline structures of the semicokes were investigated by XRD. X-ray diffraction  
19 patterns of semicokes produced after 2 hours of pyrolysis of Pitch A and Pitch B at 500°C, 700°C,  
20 and 1000°C are shown in Fig. 11 a, b, c and Fig. 11 d, e, f, respectively. In all of the patterns  
21 there is a broad peak at  $2\theta \approx 25.0^\circ$ - $25.7^\circ$ , corresponding to (002) reflection of carbon structures  
22 due to the stacking of aromatic layers.<sup>17</sup> A less defined (10) band at  $2\theta \approx 43^\circ$  in some of the  
23 patterns is also observed. On the other hand, there is a band for values of  $2\theta$  lower than the (002)  
24 peak, which has been previously described by other authors [29] for carbonaceous precursors such  
25 as lignin, and which was labelled as  $\gamma$  zone.

26 According to Alvarez et al. [30], the (002) peak is associated to the ordering of the mesogen  
27 molecules constituting the mesophase, whereas the distribution of intensities in the  $\gamma$  zone is  
28 associated to the isotropic material, which includes premesogenic structures and / or non-aromatic  
29 structures (polynaphthenic or aliphatic) as a previous stage to the formation of mesophase. Both the  
30 (002) peak and the  $\gamma$  zone are sensitive to the changes occurring during carbonization and to the  
31 mesophase growth. Consequently, our analysis of the diffractograms was centred in the range of  
32  $2\theta$  from 10 to  $35^\circ$ .

33 The broadness of the (002) peaks indicated that samples were highly amorphous [31] and  
34 there was a possible presence of crystallites perpendicular to aromatic layers [17]. At high  
35 temperatures like 1000°C, the intensity of the (002) peak clearly increased. The possible reason  
36 for this was the increasing crystalline structure at higher heat treatments. The diffraction pattern of  
37 all samples were similar to the pattern of graphite, however the intensity of the (002) peaks were  
38 so low that it indicates that the samples were probably very poor in crystalline structure. The  
39 Raman results were supporting the poor crystallinity in the carbonaceous materials, this  
40  
41  
42  
43  
44  
45  
46  
47  
48  
49  
50  
51  
52  
53  
54  
55  
56  
57  
58  
59  
60  
61  
62  
63  
64  
65

phenomenon the carbonaceous materials was due to the possible turbostratic structures leading to broad peaks of (002).

The crystallinity of the amorphous carbonaceous materials were estimated with respect to pure graphite. By using the ratio of the (002) peak area of a perfect graphite and area of the (002) peak of the samples relative to their masses, crystallinity values were determined. The results for the crystallinity estimations of semicokes obtained from of Pitch A and Pitch B are presented in Fig. 12 a and b, respectively. 0.84 was the highest percentage of crystallinity obtained from the pyrolysis of Pitch A at 1000 °C after 2 hours whereas 0.10 was the lowest percentage of crystallinity obtained from the semicokes of Pitch A at 500°C after 30 minutes, Fig. 12 a. For semicokes of Pitch B, 0.49 and 0.12 were the highest and lowest percentages of crystallinity. The highest value were obtained at 1000°C after 2 hours and the lowest one was obtained at 500 °C after 30 minutes of pyrolysis, Fig. 12 b. These graphs supported the previous arguments of increasing crystalline structure at with increasing temperature and duration of heat treatment. For both pyrolysis processes of Pitch A and Pitch B, the same trends were observed. In addition, the semicokes obtained from pyrolysis of Pitch A contained more crystalline material after treatment at high temperatures. However, around 700 °C almost same crystallinity percentage obtained from both of the feedstock. Interestingly, at temperature lower than 700 °C, semicokes of Pitch A had slightly lower crystallinity than semicokes of Pitch B.

XRD patterns obtained of the semicokes from the pyrolysis of Pitch A and Pitch B under different durations and temperatures were analyzed to obtain the structural parameters like FWHM,  $L_c$ , and  $d_{002}$  in order to make estimations on changing number of graphene layers with respect to varying conditions. Table 5 presents change of interlayer distances,  $d_{002}$ , of pitch A and pitch B products with respect to temperature and pyrolysis time. The interlayer spacing,  $d_{002}$ , with respect to temperature and time of the pyrolysis reactions of pitch A changed in the range of 0.346-0.356 nm, where as  $d_{002}$ , of pitch B changed in the range of 0.347-0.362 nm, respectively.

However, a correlation between  $d_{002}$  values and pyrolysis parameters could not be done due to the turbostratic structure of the semicokes and complex structure of the pitches. Also, the comparison of  $d_{002}$  of semicokes of pitch A and B for 2 hours pyrolysis indicated that there was not a correlation between  $d_{002}$  values and these pitch types. Generally, heat treatment of carbons below 1800°C results in very disordered carbons containing turbostratic structures. The presences of local stacking faults, random shifting between layers, unorganized carbon structures, strain in the layers, and unsteady interlayer spacings are the main reasons for the disorder [17]. For this reason the results presented in the graphs with respect to change in time, temperature, and pitch

1  
2  
3  
4  
5  
6  
7  
8  
9  
10  
11  
12  
13  
14  
15  
16  
17  
18  
19  
20  
21  
22  
23  
24  
25  
26  
27  
28  
29  
30  
31  
32  
33  
34  
35  
36  
37  
38  
39  
40  
41  
42  
43  
44  
45  
46  
47  
48  
49  
50  
51  
52  
53  
54  
55  
56  
57  
58  
59  
60  
61  
62  
63  
64  
65

type were the signs of high disorder probably caused by the turbostratic structures in hydrographenes materials.

Fig. 13 shows the effect of temperature and duration on the number of graphene layers for semicokes of Pitch A. In addition to that, in Fig. 14, a comparison of layer numbers between semicokes of Pitch A and Pitch B can be seen. In these figures, average numbers of graphene layers,  $n$ , were calculated by using classic Debye-Scherer equation. However, calculated stacking height,  $L_c$ , and the number of layers were not exactly equal to exact values of the crystallites because these equations can only be derived for highly graphitized carbon materials [17]. Therefore, these equations are not suitable for highly turbostratic carbons because the positive interference function from intralayer plane is too strong to be cancelled by the negative interference function, which becomes weak in carbon layers with small numbers of stacking [32]. For that reason, calculated values of  $n$  were used as a convenient relative estimate of actual crystallite sizes and layer numbers that were probably greater than the calculated values. Fig. 13 presents the calculated average  $n$  values that are changing between 5-10 graphene layers. Although, there was not any distinct correlation between experimental conditions and the calculated results,  $n$  values were 5 to 7 layers at temperature higher than 700°C and 7 to 10 at temperatures 500-600°C. The calculated values of average  $n$  are similar to values measured for pyrolyzed lignin forming turbostratic carbons [17], and number of layers in turbostratic carbons simulated by Yang and Frindt [33]. Other than duration and temperature effects on  $n$  values, type of pitches seemed to affect the calculated values as presented in Fig. 14. More specifically, semicokes seemed to have fewer layers in case of Pitch B when compared with the semicokes obtained from Pitch A.

### 3.2.5. Scanning electron microscopy of the semicokes

SEM images of the semicokes obtained from the pyrolysis of Pitch A at 600°C after two hours are presented in Fig. 15. Physical appearances of semicokes were quite different in different spots during the analyses. The SEM photographs clearly indicated that there was formation of pores and layering structure during the heat treatment process. The formation of pores was due to the devolatilization reactions taking place in the pyrolysis process. The effect of increasing the temperature were also examined by SEM. SEM micrographs of the semicokes produced at 700°C shows different morphology than the semicokes at lower temperatures, Fig. 16. Both images at low and high magnifications clearly show the formation of turbostratic structures and expansion of carbon layers [17]. Fig. 17 represents the morphologies of semicokes when the pyrolysis

1  
2  
3  
4  
5  
6  
7  
8  
9  
10  
11  
12  
13  
14  
15  
16  
17  
18  
19  
20  
21  
22  
23  
24  
25  
26  
27  
28  
29  
30  
31  
32  
33  
34  
35  
36  
37  
38  
39  
40  
41  
42  
43  
44  
45  
46  
47  
48  
49  
50  
51  
52  
53  
54  
55  
56  
57  
58  
59  
60  
61  
62  
63  
64  
65

temperature was increased to 800°C. The micrographs demonstrated that there was an increase in the turbostratic content in semicokes at higher temperatures.

#### 4. Conclusion

The consistent results of both FTIR and solid-state <sup>13</sup>C-NMR spectra proved that aromatic structure formation in the semicokes was favored with increasing pyrolysis temperature. On the other hand, comparison of FTIR spectra of semicokes with respect to pyrolysis duration demonstrated that aromatic structure formation was also favored with increasing duration of pyrolysis due to the continuous decrease of ratio of aliphatic intensities to aromatic intensities and elimination of aliphatic groups attached to aromatic structures. Aromaticity of the carbonaceous semicokes was calculated as 0.54 and 0.64, for pitch A at 500°C after 120 minutes, and pitch B at 600°C after 120 minutes, respectively.

XRD patterns of the semicokes clearly indicated the change in the crystalline structure of solid products at various pyrolysis temperatures and durations. Percent crystallinity of semicokes products increased with increasing temperature and duration.

The D and G bands in Raman spectra demonstrated the disordered multi-layered structure, and the broadness and low intensity of (002) peak in the XRD patterns demonstrated the presence of amorphous structure of the semicokes. The effect of temperature on the crystalline structures was explained by the increase in I<sub>D</sub>/I<sub>G</sub> ratio and decrease in the intensities of D and G bands indicating a decrease in the disorder of the semicokes with increasing pyrolysis temperature.

Decrease in the intensity of the G bands with increasing temperature indicated there might be a decrease in the number of layers in semicokes. The calculated average numbers of graphene layers were 5 to 7 layers at temperatures higher than 700°C and 7 to 10 at temperatures 500-600°C but there was not a distinct correlation between experimental conditions and the calculated n values. The possible reason was the small dimensions of crystallites perpendicular to aromatic layers. So the results presented for average number of layers in this work might be considered as an indication for the presence of turbostratic structures in the semicokes.

The SEM images demonstrated the semicokes contained turbostratic structures. In addition, SEM images clearly indicated the effect of increasing the temperature on the material structure. Semicokes produced at higher pyrolysis temperatures had turbostratic

1 structures and the expansion of carbon layers after the formation of layering was evidently  
2 observed.  
3  
4

## 5 **References**

6  
7

8  
9 [1] E. Fitzer, K.H. Köchling, H. Marsh, Recommended terminology for the description of  
10 carbon as a solid, *Pure Appl. Chem.* 67 (1995) 473-506.

11  
12 [2] H. Marsh, E.A. Heintz, F. Rodriguez-Reinoso, Introduction to Carbon Technologies,  
13 Universidad de Alicante, Alicante, Spain, (1997).  
14

15  
16 [3] V.G. Rocha, M. Granda, R. Santamaría, C. Blanco, E.I. Diestre, R. Menéndez, Pyrolysis  
17 behaviour of pitches modified with different additives, *J. Anal. Appl. Pyrolysis* 73 (2005)  
18 276-283.  
19

20  
21 [4] V. Slovák, P. Susàk, Pitch pyrolysis kinetics from single TG curve, *J. Anal. Appl.*  
22 *Pyrolysis* 72 (2000) 249-252.  
23

24  
25 [5] H. Marsh, M. Martínez-Escandell, F. Rodríguez-Reinoso, Semisemicokes from pitch  
26 pyrolysis: mechanisms and kinetics, *Carbon* 37 (1999) 363-390.  
27

28  
29 [6] J.K. Brown, P.B. Hirsch, Recent infra-red and X-ray studies of coal, *Nature* 175 (1955)  
30 229–233.  
31

32  
33 [7] L.G. Kuzmina, A.V. Churakov, J.A.K. Howard, A.I. Vedernikov, N.A. Lobova, A.A.  
34 Botsmanova, M.V. Alfimov, S.P. Gromov, Structural investigation of model compounds for  
35 an acceptor component of a new type of charge-transfer complexes based on  
36 viologen analogues. Characteristic features of the molecular and supramolecular structures,  
37 *Crystallogr. Rep.* 50 (2005) 234–253.  
38

39  
40 [8] R.P. Suggate, W.W. Dickinson, Carbon NMR of coals: The effects of coal type and rank,  
41 *Int. J. Coal Geol.* 57 (2004) 1–22.  
42

43  
44 [9] P. Conte, R. Spaccini, A. Piccolo, A. State of the art of CPMAS <sup>13</sup>C-NMR spectroscopy  
45 applied to natural organic matter. *Prog. Nucl. Magn. Reson. Spectrosc.* 44 (2004) 215–223.  
46

47  
48 [10] T. Takanohashi, H. Kawashima, Construction of a model structure for Upper Freeport  
49 coal using <sup>13</sup>C NMR chemical shift calculations, *Energy Fuels* 16 (2002) 379–387.  
50

51  
52 [11] X.Y. Cao, M.A. Chappell, A. Schimmelmann, M. Mastalerz, Y. Li, W.G. Hu, J.D. Mao,  
53 Chemical structure changes in kerogen from bituminous coal in response to dike intrusions as  
54 investigated by advanced solid-state C-13 NMR spectroscopy, *Int. J. Coal Geol.* 108 (2013)  
55 53–64.  
56  
57  
58  
59

- 1  
2 [12] X.Y. Cao, J. Yang, J.D. Mao, Characterization of kerogen using solid-state nuclear  
3 magnetic resonance spectroscopy: A review, *Int. J. Coal Geol.* 108 (2013) 83–90.  
4 [13] J. Cerny, Structural dependence of CH bond absorptivities and consequences for FT-IR  
5 analysis of coals, *Fuel* 75 (1996) 1301–1306.  
6 [14] W. Geng, T. Nakajima, H. Takanashi, A. Ohki, Analysis of carboxyl group in coal and  
7 coal aromaticity by Fourier transform infrared spectrometry, *Fuel* 88 (2009) 139–144.  
8 [15] W.-t. Cho, S. Kim, H.-k. Choi, Y.-j. Rhim, J.-h. Lim, S.-h. Lee, J. Yoo, Characterization  
9 of chars made of solvent extracted coals, *Korean J. Chem. Eng.* 29 (2012) 190–195.  
10 [16] W. Dun, L. Guijian, S. Ruoyu, F. Xiang, Investigation of structural characteristics of  
11 thermally metamorphosed coal by FTIR spectroscopy and X-ray diffraction, *Energy Fuels*  
12 27 (2013) 5823–5830.  
13 [17] B. Sakintuna, S. Çetinkaya, Y. Yürüm, Evolution of carbon microstructures during the  
14 pyrolysis of turkish elbistan lignite in the temperature range 700-1000°C, *Energy Fuels* 18  
15 (2004) 883-888.  
16 [18] H. Marsh, M. Martinez-Escandell, F. Rodriguez-Reinoso, Semisemicokes from pitch  
17 pyrolysis: mechanisms and kinetics, *Carbon* 37 (1999) 363–390.  
18 [19] G. Svehla, *Comprehensive Analytical Chemistry, Volume VI: Analytical Infrared*  
19 *Spectroscopy*, Elsevier, (1976).  
20 [20] C. Diaz, C.G. Blanco, NMR: A Powerful Tool in the Characterization of Coal Tar Pitch.  
21 *Energy Fuels* 17 (2003) 907-913.  
22 [21] Y. Yürüm, M. Azık, N. Altıntaş, E. Şanlıtürk, Characterization of the structural features  
23 of oxidized Beypazari lignite using devonvoluated solid state CNMR spectra, *Fuel*  
24 *Sci.Technol. Int'l.* 8 (1990) 917-933.  
25 [22] T. Yoshida, M. Sasaki, K. Ikeda, M. Mochizuki, Y. Nogami, Y. Inokuchi, Prediction of  
26 coal liquefaction reactivity by solid state <sup>13</sup>C NMR spectral data, *Fuel* 81 (2002) 1533-1539.  
27 [23] T.S. Bandara, K.G.S. Kannangara, M.A. Wilson, The study of Australian coal maturity:  
28 relationship between solid-state NMR aromaticities and organic free-radical count, *Energy*  
29 *Fuels* 19 (2005) 954-959.  
30 [24] X. Gong, Z. Guo, Z. Wang, Variation of char structure during anthracite pyrolysis  
31 catalyzed by Fe<sub>2</sub>O<sub>3</sub> and its influence on char combustion reactivity, *Energy Fuels* 23 (2009)  
32 4547-4552.  
33 [25] A.C. Ferrari, J.C. Meyer, Raman spectrum of graphene and graphene layers, *Phys. Rev.*  
34 *Lett.* 97 (2006).

- 1  
2 [26] A.C. Ferrari, Raman spectroscopy of graphene and graphite: disorder, electron-phonon  
3 coupling, doping and nonadiabatic effects, *Solid State Comm.* 143 (2007) 47-57.  
4 [27] D. Graf, F. Molitor, K. Ensslin, C. Stampfer, A. Jungen, C. Hierold, L. Wirtz,  
5 Spatially resolved raman spectroscopy of single and few-layer grapheme, *Nano Letters* 7  
6 (2007) 238-242.  
7 [28] H. Wang, Y. Wu, C.K.S. Choong, J. Zhang, K.L. Teo, Z. Ni, Z. Shen, Disorder Induced  
8 Bands in First Order Raman Spectra of Carbon Nanowalls, 6th IEEE Conf. Nanotechnology  
9 1 (2006) 219-222.  
10 [29] V.I. Saranchuck, L.V. Pashchenko, T.G. Shendrik, L.Y.A. Galushko, In: Extended  
11 Abstracts, Carbon'96, Newcastle upon Tyne, UK: The British Carbon Group, pp. 435-436  
12 (1996).  
13 [30] A.G. Alvarez , M. Martinez-Escandell, M. Molina-Sabio, F. Rodriguez-Reinoso,  
14 Pyrolysis of petroleum residues: analysis of semicokes by X-ray diffraction, *Carbon* 37 (1999)  
15 1627-1632.  
16 [29] R.A. Greinke, L.S. Singer, Constitution of coexisting phases in mesophase pitch during  
17 heat treatment: mechanism of mesophase formation, *Carbon* 26 (1988) 665-670.  
18 [32] H. Fujimoto, Theoretical x-ray scattering intensity of carbons with turbostratic stacking  
19 and AB stacking structures, *Carbon* 41 (2003) 1585-1592.  
20 [33] D. Yang, R.P. Frindt, Powder x-ray diffraction of turbostratically stacked layer systems,  
21 *J. Matter. Res.* 11 (1996) 1777-1781.  
22  
23  
24  
25  
26  
27  
28  
29  
30  
31  
32  
33  
34  
35  
36  
37  
38  
39  
40  
41  
42  
43  
44  
45  
46  
47  
48  
49  
50  
51  
52  
53  
54  
55  
56  
57  
58  
59  
60  
61  
62  
63  
64  
65

## Captions of Figures

**Fig. 1.** Yields of semicokes of a) Pitch A and b) Pitch B with respect to pyrolysis temperature and time

**Fig. 2.** FTIR spectra of a) Pitch A and b) Pitch B

**Fig. 3.** FTIR spectra of semicokes obtained from pyrolysis of pitch A after 120 min at a) 500°C, b) 900°C and from pyrolysis of Pitch B after 120 min at c) 600°C, d) 1000°C

**Fig. 4.** FTIR spectra of semicokes from pyrolysis of Pitch A at 800°C for a) 30 min, b) 60 min and c) 120 min

**Fig. 5.** <sup>1</sup>H-NMR spectra of a) Pitch A and b) Pitch B

**Fig. 6.** Solid-state <sup>13</sup>C-NMR spectra of semicokes of Pitch A for 120 min hours at a) 500°C, b) 600°C, c) 700°C, d) 800°C, and e) 900°C

**Fig. 7.** Solid-state <sup>13</sup>C-NMR spectra of semicokes of Pitch B for 120 min at a) 600°C, b) 800°C, and c) 1000°C

**Fig. 8.** Deconvoluted solid state <sup>13</sup>C NMR spectra of semicokes from pyrolysis of a) Pitch A at 500°C for 120 min, b) Pitch B at 600°C for 120 min

**Fig. 9.** Raman spectra of semicokes of a) Pitch A for 120 min at 500, 700 and 900°C and b) Pitch B for 120 min at 500, 700 and 1000°C

**Fig. 10.** Raman spectra of semicokes of Pitch A at a) 900°C and b) 500°C for 30, 60 and 120 min

**Fig. 11.** X-ray diffraction pattern of semicokes produced from Pitch A pyrolysis for 120 min at a) 500 °C, b) 700 °C, and c) 1000 °C, and from from Pitch B pyrolysis for 120 min at d) 500 °C, e) 700 °C, and f) 1000 °C

**Fig. 12.** Crystallinity of semicokes from pyrolysis of a) Pitch A and b) Pitch B

**Fig. 13.** Calculated *n* values of semicokes of Pitch A with respect to time and temperature

**Fig. 14.** Change in calculated *n* values of semicokes at 120 min pyrolysis with respect to pitch type and pyrolysis temperature

**Fig. 15.** SEM micrographs of semicokes of Pitch A obtained at 600 °C for 120 min showing a) pores and b) layering structures

**Fig. 16.** SEM micrographs of semicokes of Pitch A obtained at 700 °C for 120 min showing a) turbostratic structures and b) expansion of layers

**Fig. 17.** SEM micrographs of semicokes of Pitch A obtained at 800 °C for 120 min showing high turbostratic structure content at a) 15KX and b) 60KX magnifications

## Legends of Tables

### Table 1

Elemental analysis data for Pitch A and Pitch B, wt %.

### Table 2

Percent areas of functional groups calculated from the deconvoluted  $^{13}\text{C}$  NMR spectra of the carbonaceous solid residues obtained from Pitch A and Pitch B.

### Table 3

Parameters of D Band.

### Table 4

Parameters of G Band.

### Table 5

Interlayer distances,  $d_{002}$ , of Pitch A and Pitch B semicokes with respect to temperature and pyrolysis time.

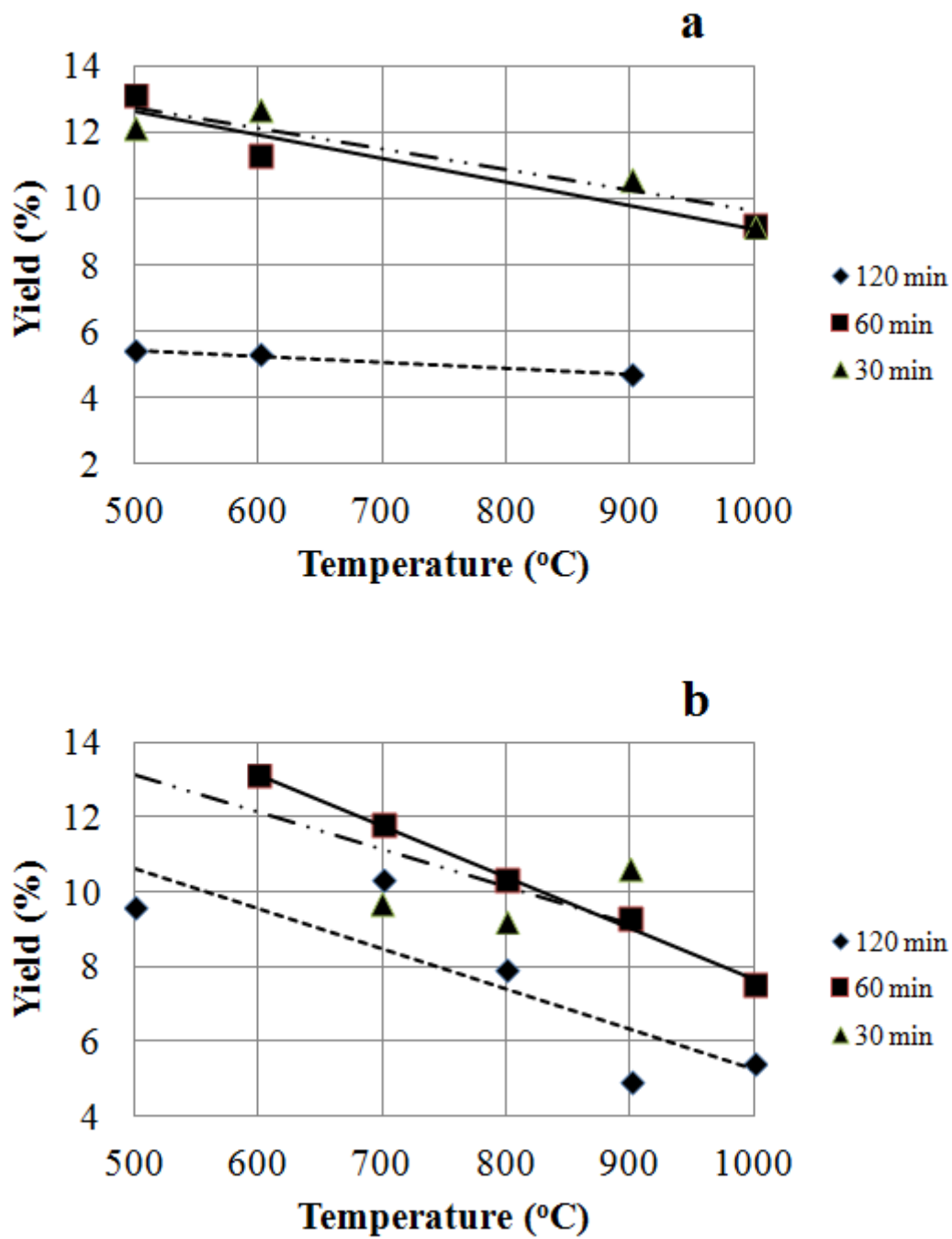


**Fig. 1.** Yields of semicokes of a) Pitch A and b) Pitch B with respect to pyrolysis temperature and time.

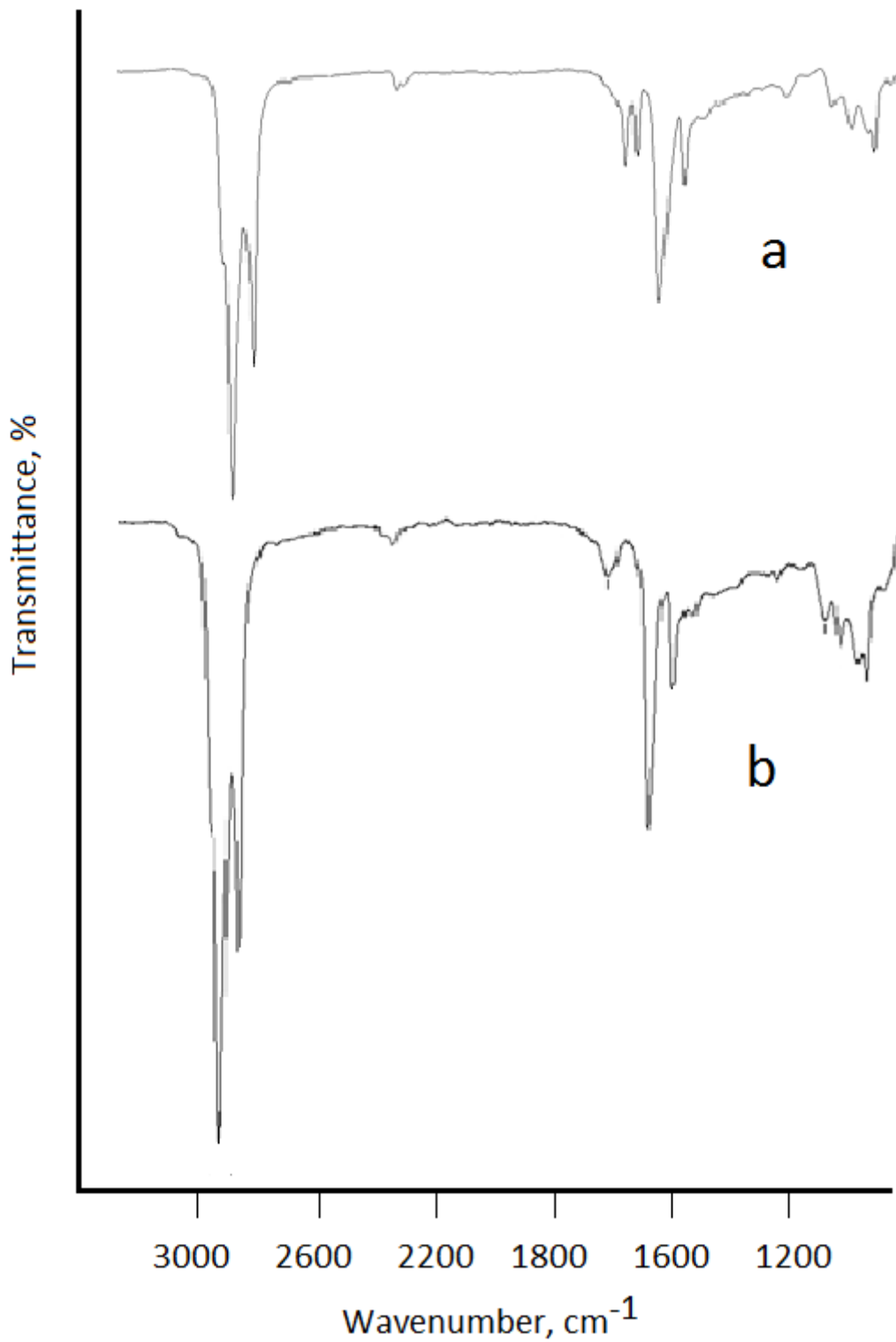
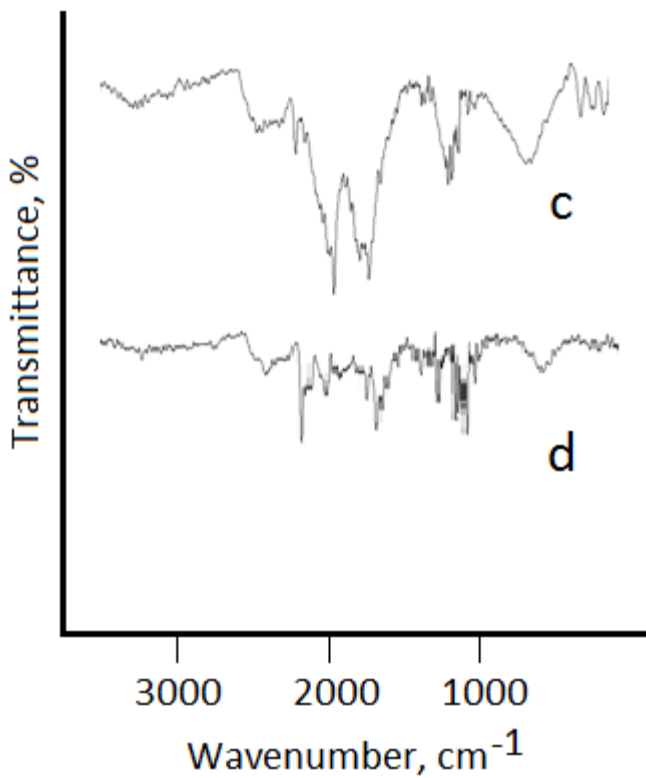
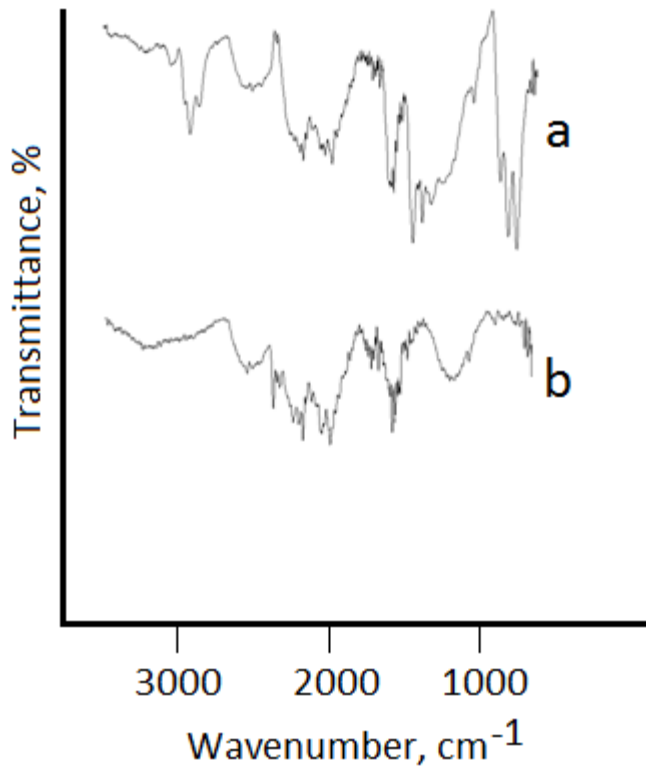


**Fig. 2.** FTIR spectra of a) Pitch A and b) Pitch B.



57 **Fig. 3.** FTIR spectra of semicokes obtained from pyrolysis of Pitch A after 120 min at  
58 a) 500°C, b) 900°C and from pyrolysis of Pitch B after 2h at c) 600°C, d) 1000°C.  
59

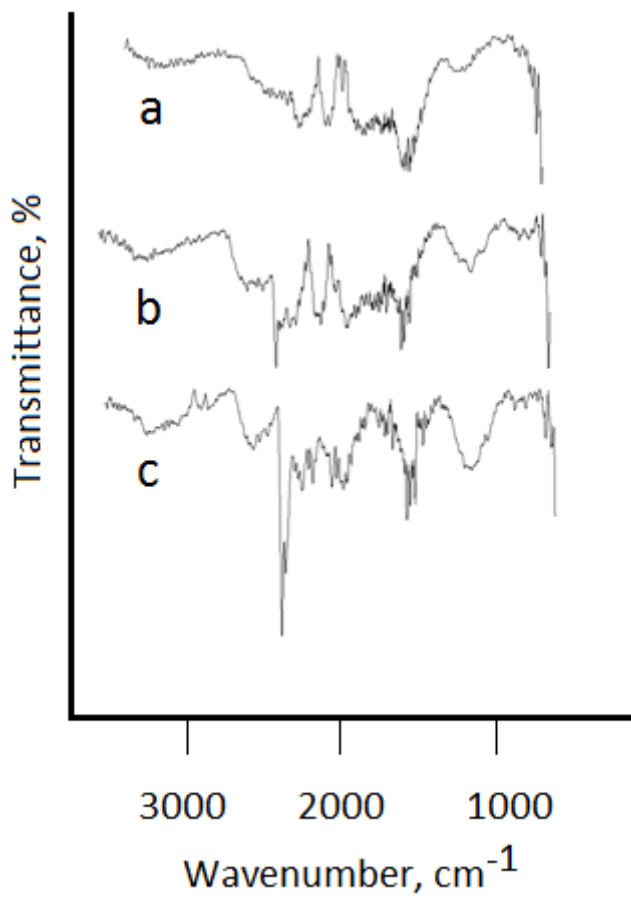


**Fig. 4.** FTIR spectra of semicokes from pyrolysis of Pitch A at 800°C for a) 30 min, b) 60 min and c) 120 min.

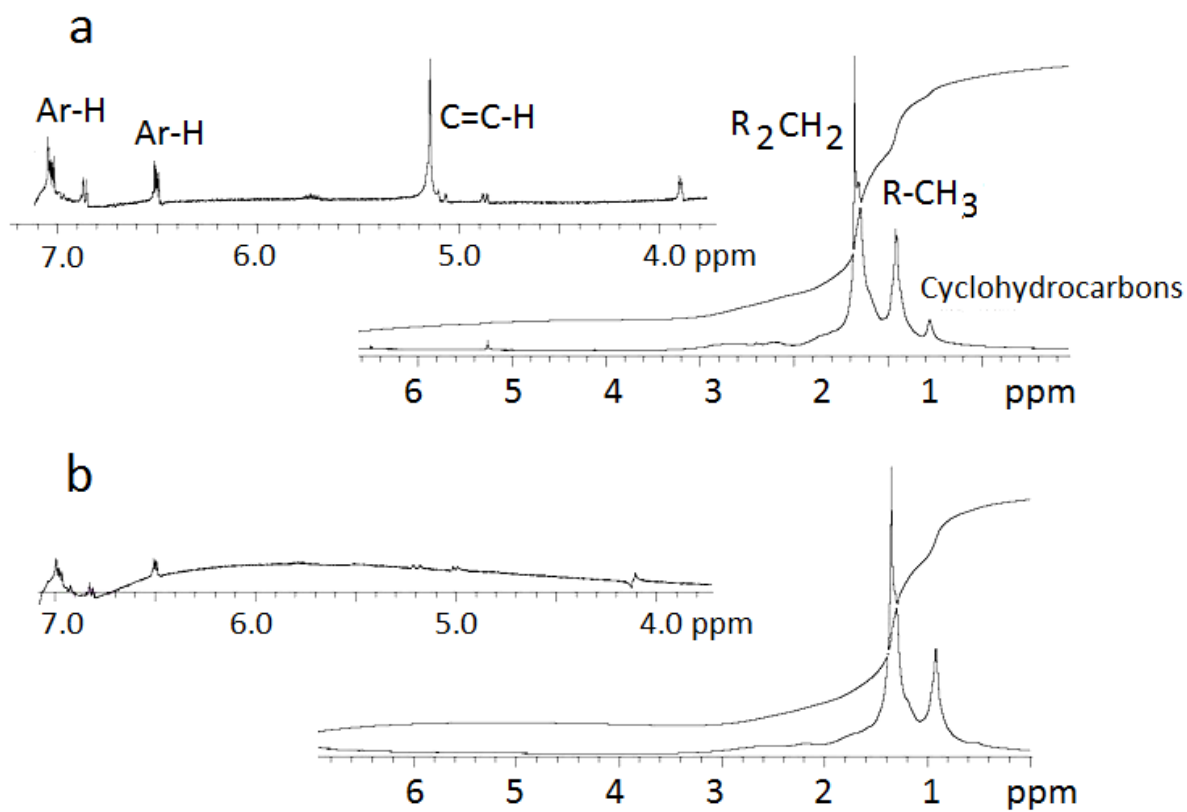


**Fig. 5.** <sup>1</sup>H-NMR spectra of a) Pitch A and b) Pitch B.

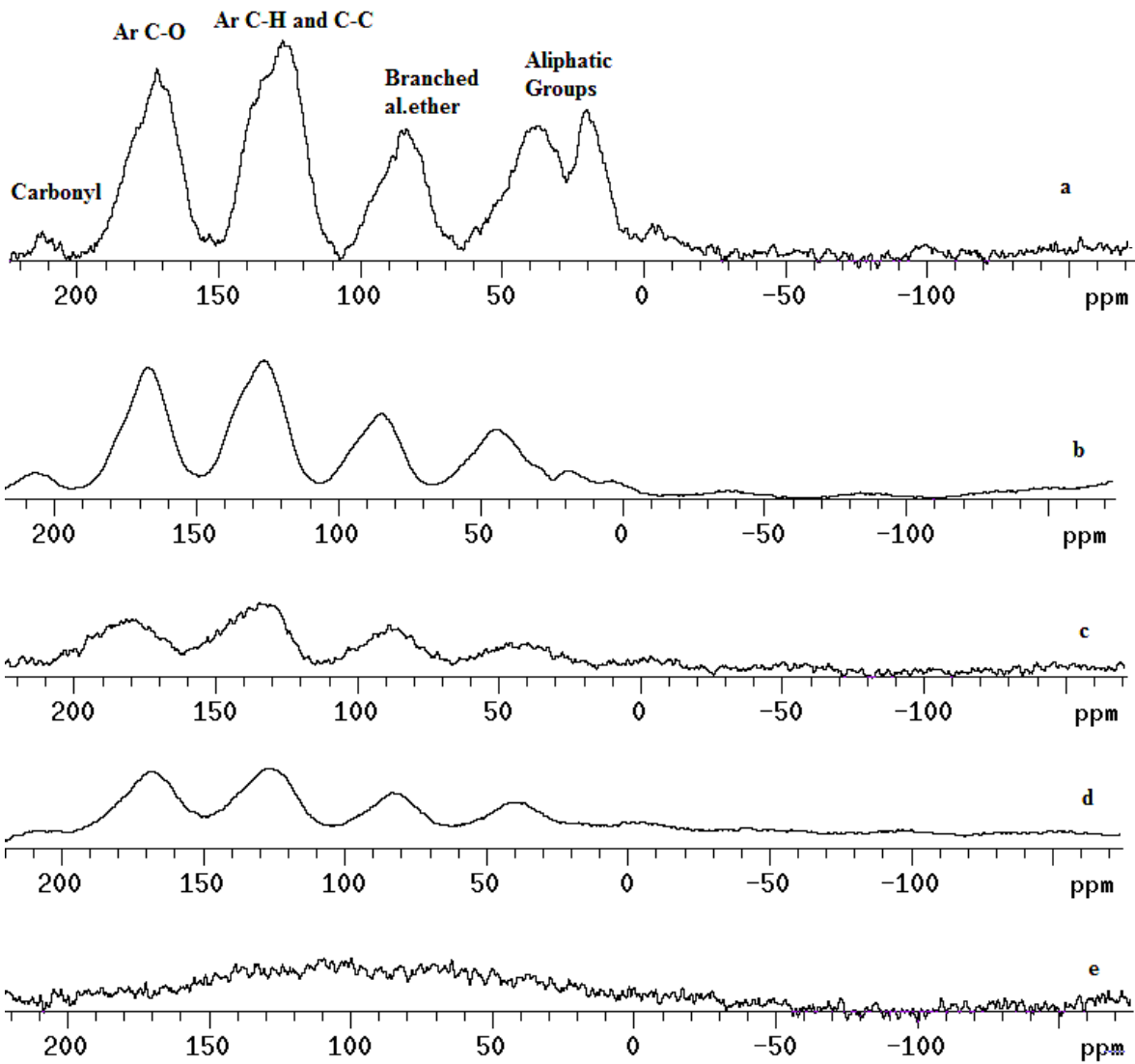


**Fig. 6.** Solid-state  $^{13}\text{C}$ -NMR spectra of semicokes of Pitch A for 120 min at a) 500°C, b) 600°C, c) 700°C, d) 800°C, and e) 900°C.

1  
2  
3  
4  
5  
6  
7  
8  
9  
10  
11  
12  
13  
14  
15  
16  
17  
18  
19  
20  
21  
22  
23  
24  
25  
26  
27  
28  
29  
30  
31  
32  
33  
34  
35  
36  
37  
38  
39  
40  
41  
42  
43  
44  
45  
46  
47  
48  
49  
50  
51  
52  
53  
54  
55  
56  
57  
58  
59  
60  
61  
62  
63  
64  
65

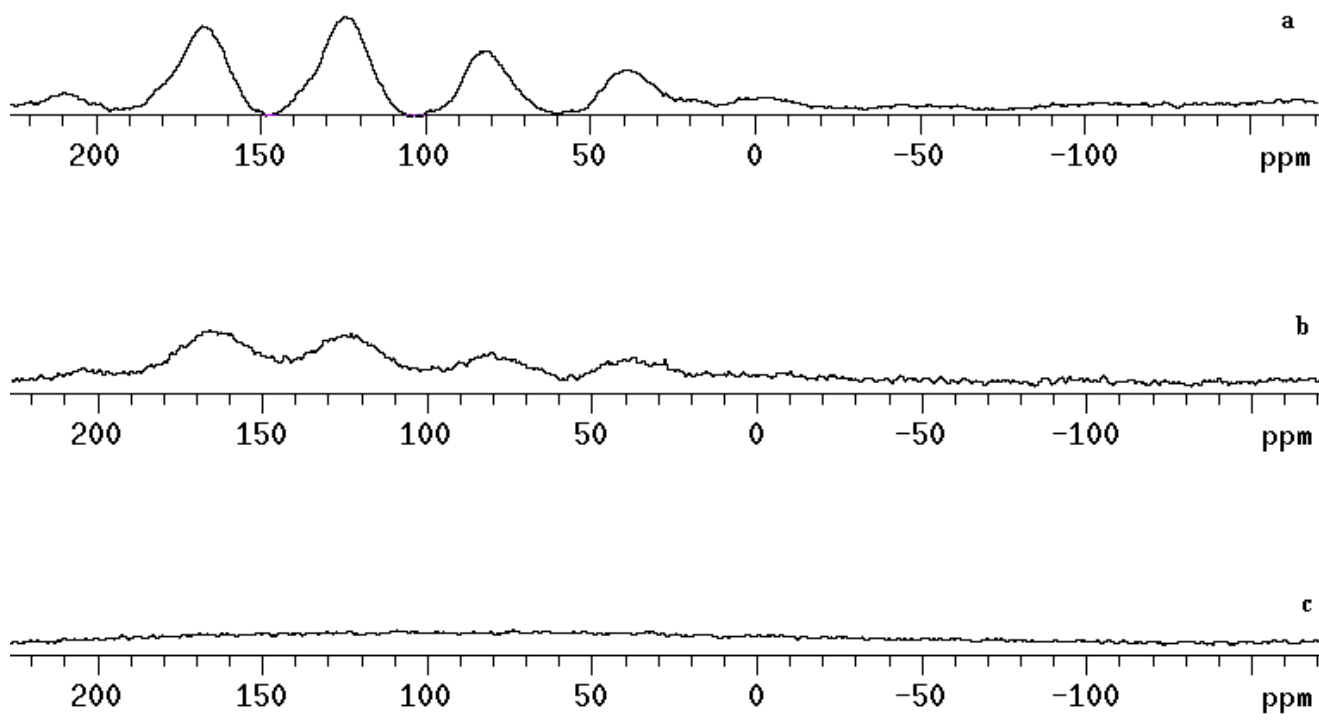


**Fig. 7.** Solid-state <sup>13</sup>C-NMR spectra of semicokes of Pitch B for 120 min at a) 600°C, b) 800°C, and c) 1000°C.

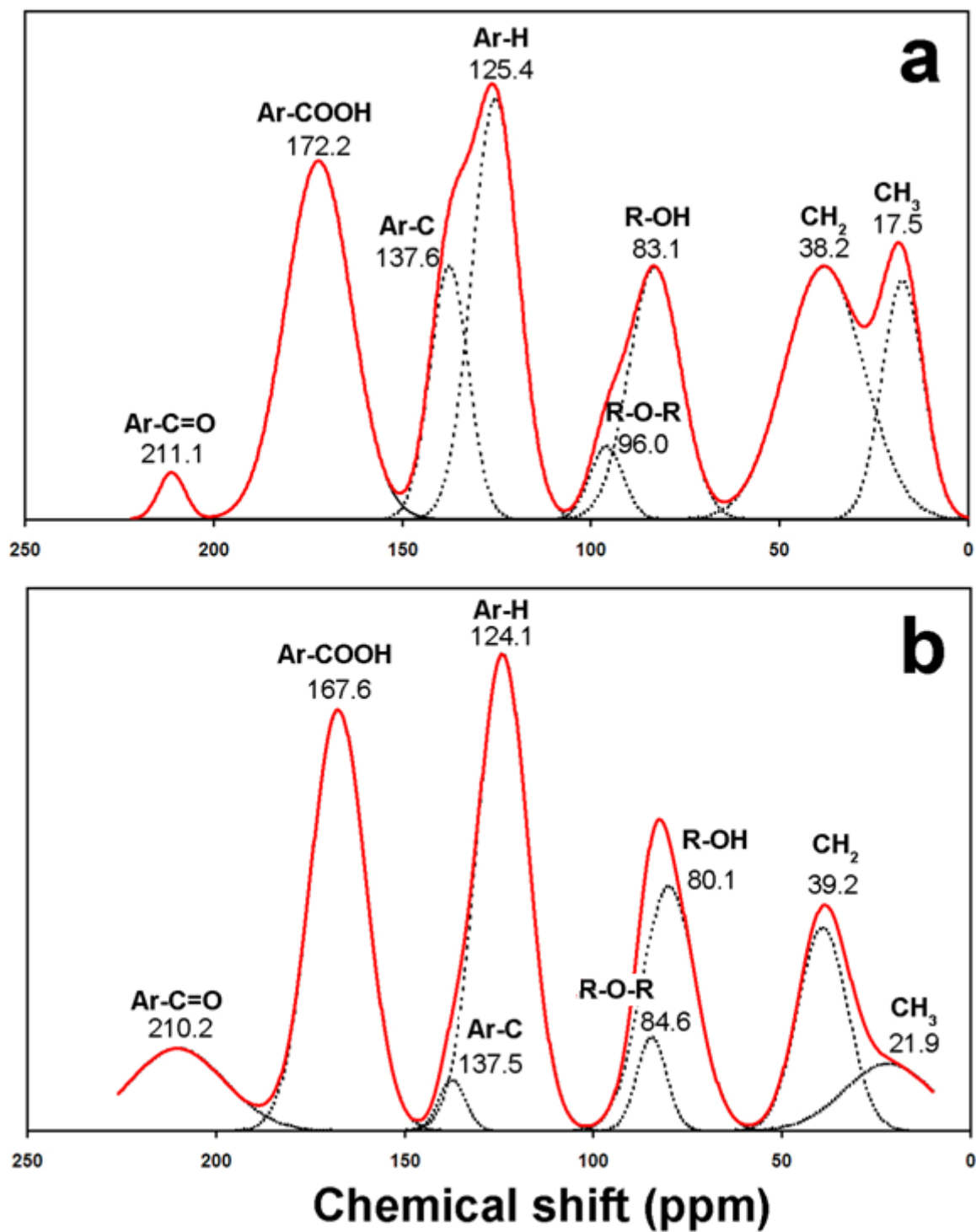


**Fig. 8.** Deconvoluted solid state <sup>13</sup>C NMR spectra of semicokes from pyrolysis of a) Pitch A at 500°C for 120 min, b) Pitch B at 600°C for 120 min.

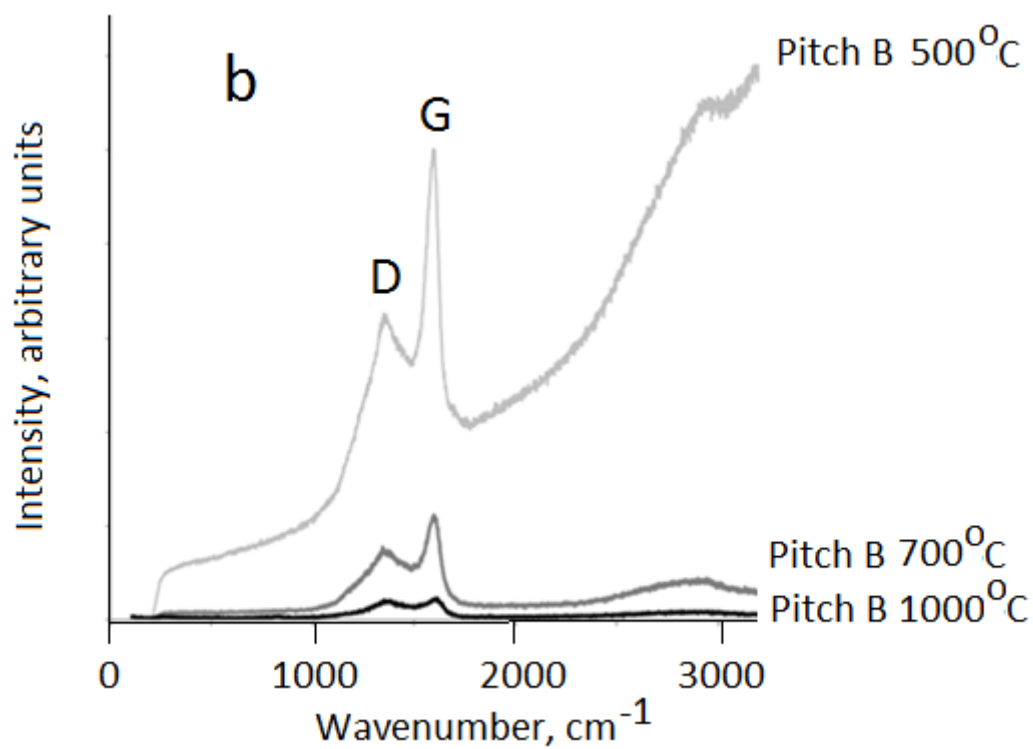
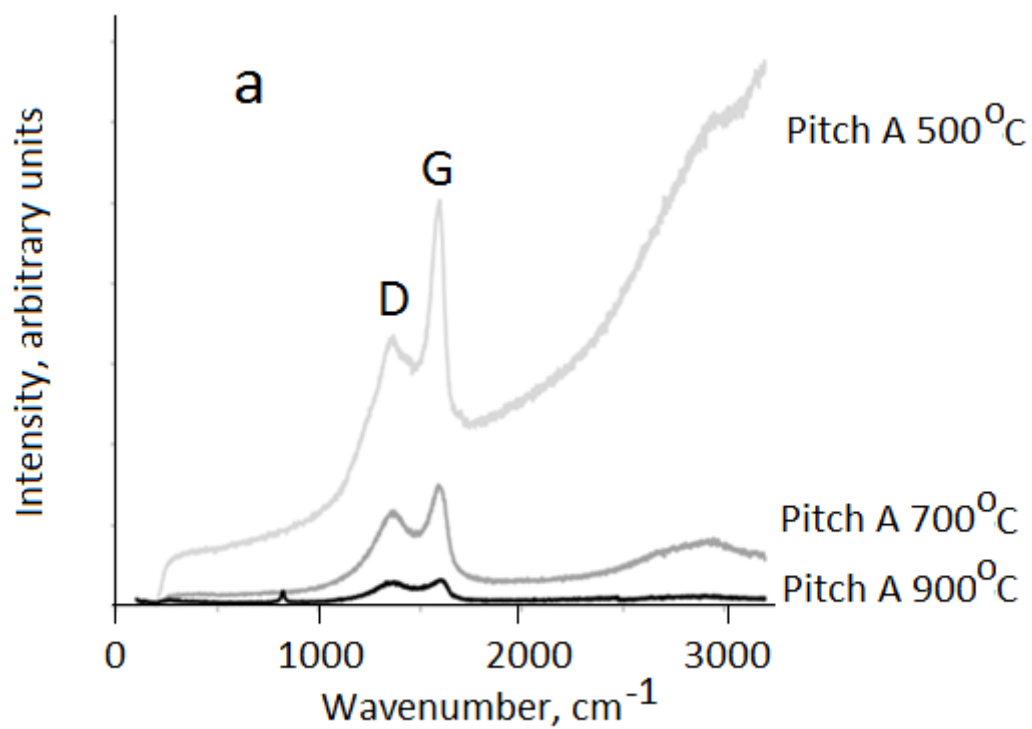


**Fig. 9.** Raman spectra of semicokes of a) Pitch A for 120 min at 500, 700 and 900°C and b) Pitch B for 120 min at 500, 700 and 1000°C.

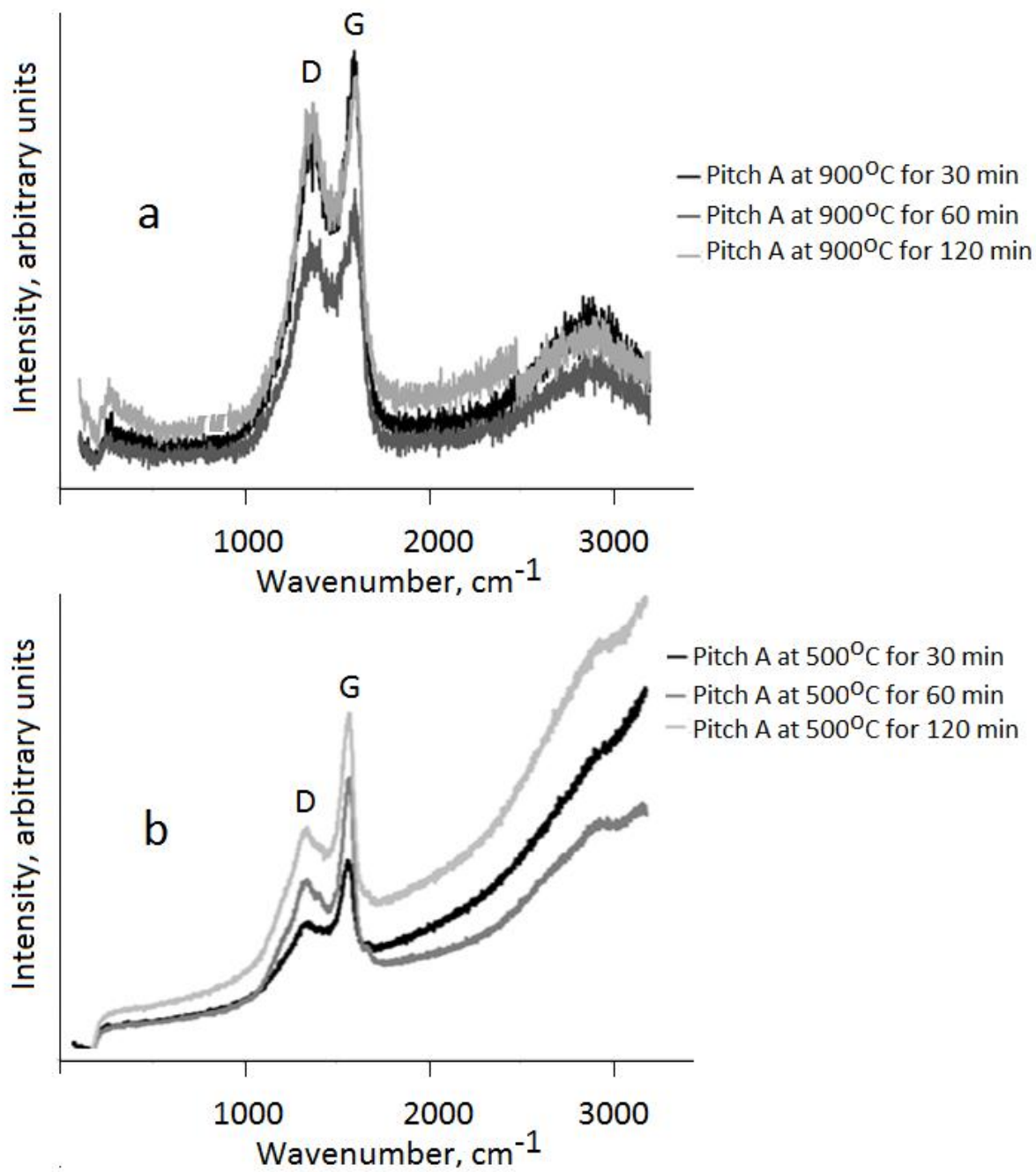


**Fig. 10.** Raman spectra of semicokes of Pitch A at a) 900°C and b) 500°C for 30, 60 and 120 min.

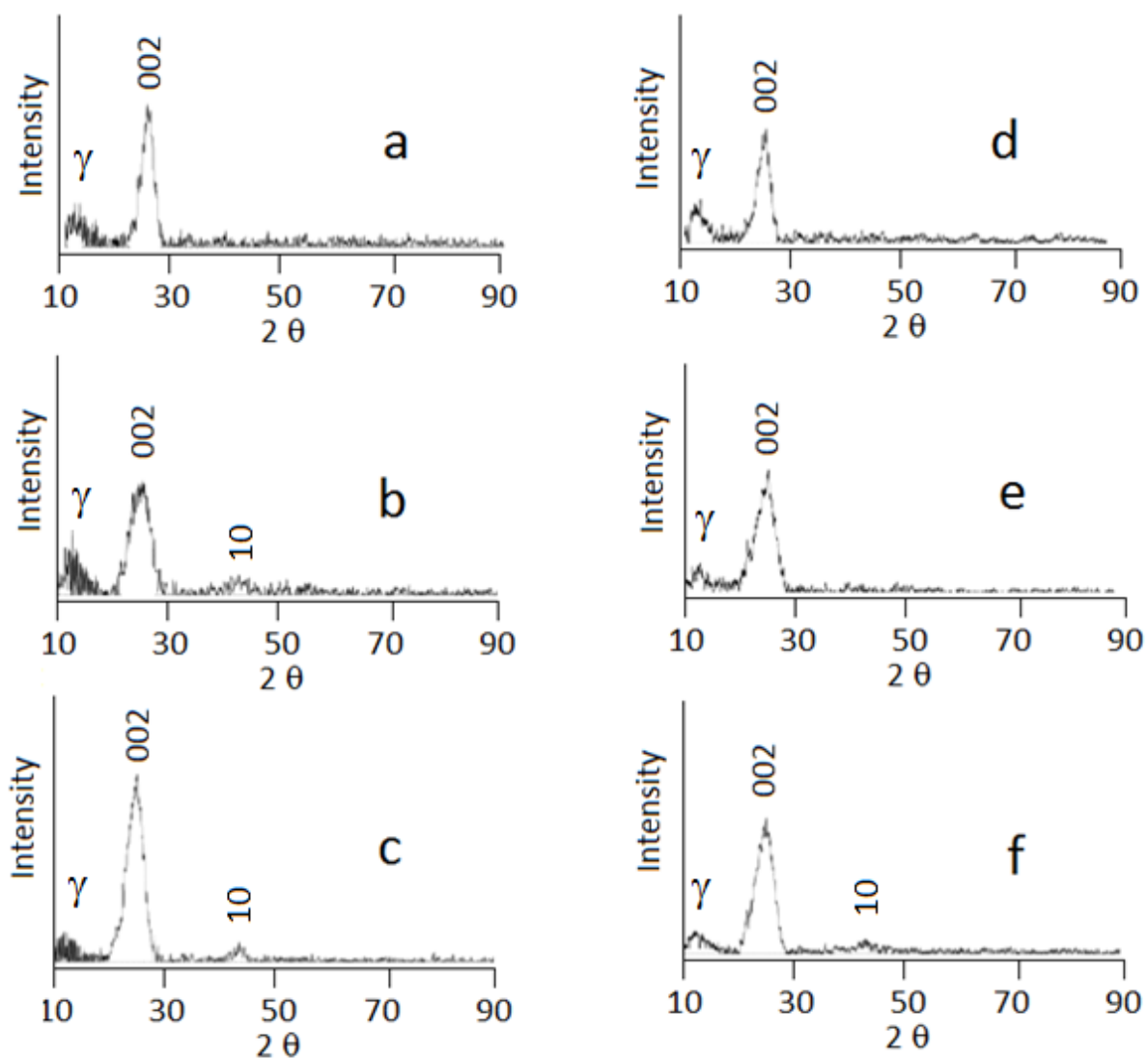


**Fig. 11.** X-ray diffraction pattern of semicokes produced from Pitch A pyrolysis for 120 min at a) 500°C, b) 700°C, and c) 1000°C, and from from Pitch B pyrolysis for 120 min at d) 500°C, e) 700°C, and f) 1000°C.

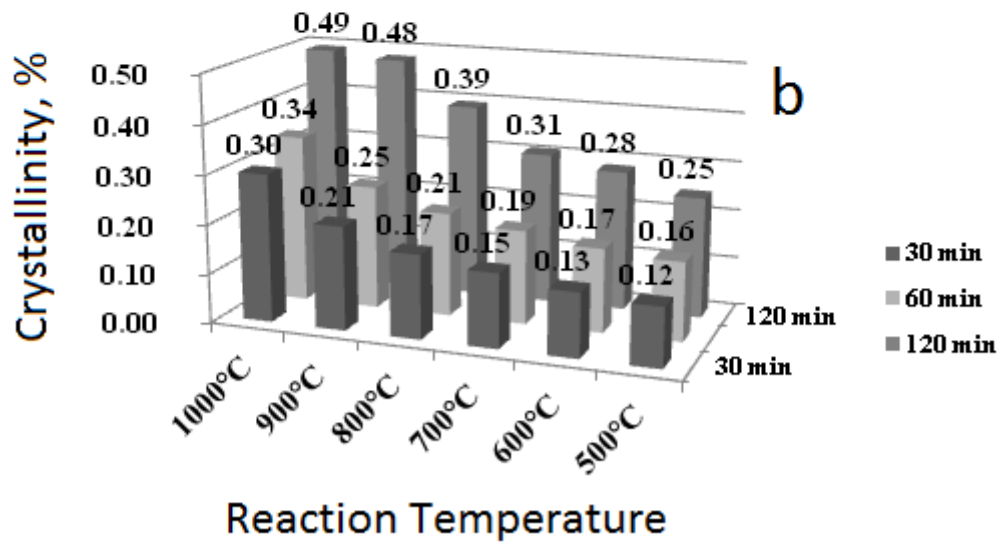
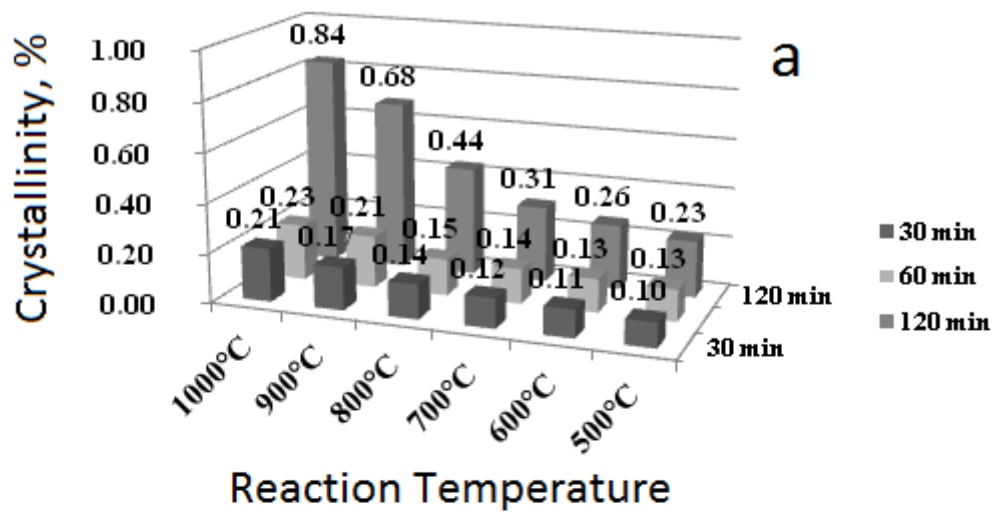


**Fig. 12.** Crystallinity of semicokes from pyrolysis of a) Pitch A and b) Pitch B.

1  
2  
3  
4  
5  
6  
7  
8  
9  
10  
11  
12  
13  
14  
15  
16  
17  
18  
19  
20  
21  
22  
23  
24  
25  
26  
27  
28  
29  
30  
31  
32  
33  
34  
35  
36  
37  
38  
39  
40  
41  
42  
43  
44  
45  
46  
47  
48  
49  
50  
51  
52  
53  
54  
55  
56  
57  
58  
59  
60  
61  
62  
63  
64  
65

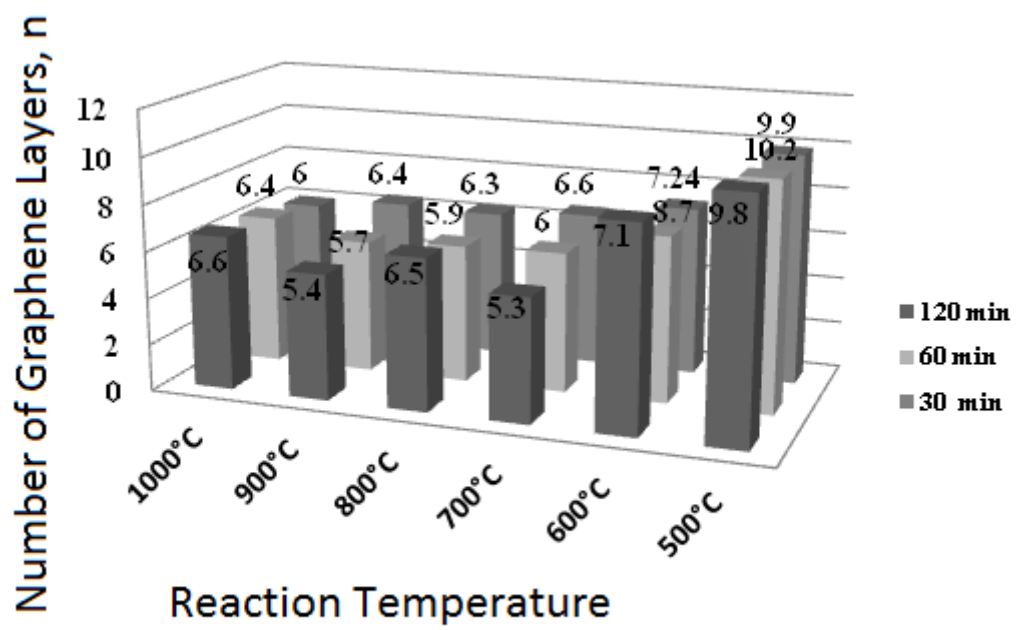


**Fig. 13.** Calculated  $n$  values of semicokes of Pitch A with respect to time and temperature.

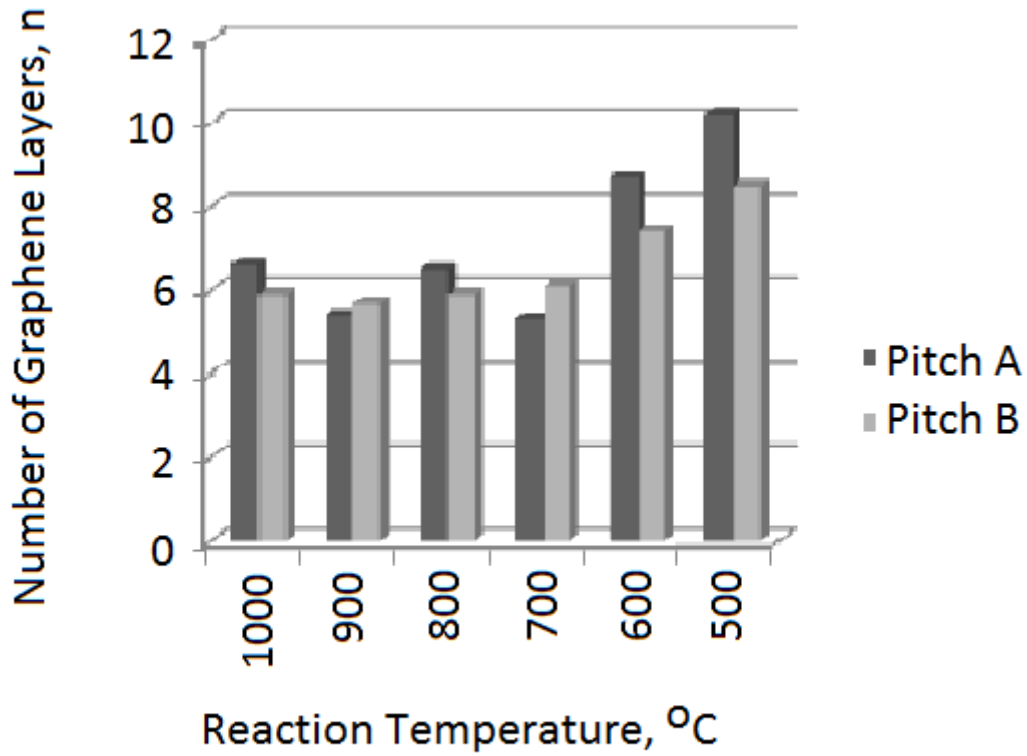


**Fig. 14.** Change in calculated  $n$  values of semicokes at 120 min pyrolysis with respect to pitch type and pyrolysis temperature.

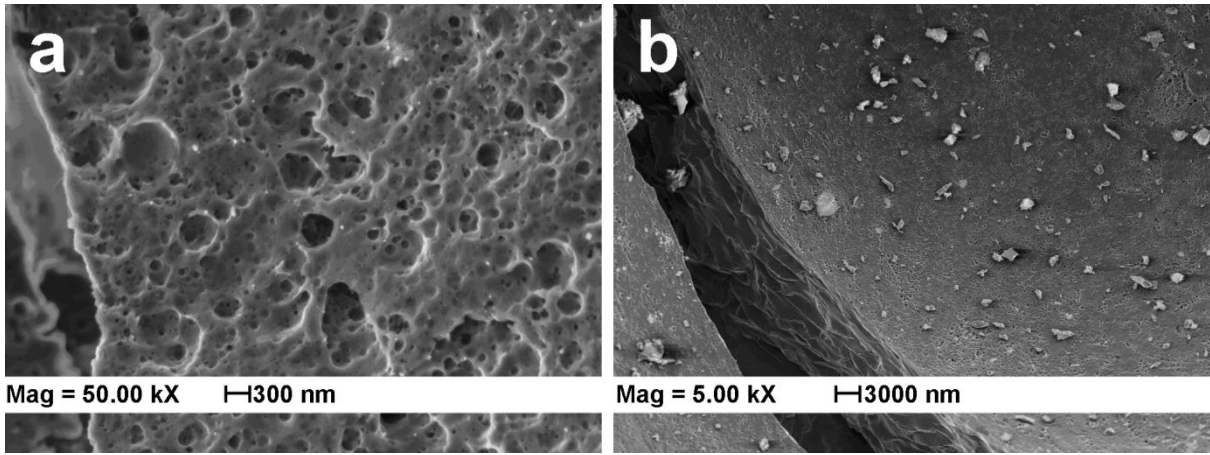


**Fig. 15.** SEM micrographs of semicokes of Pitch A obtained at 600°C for 120 min showing a) pores and b) layering structures.

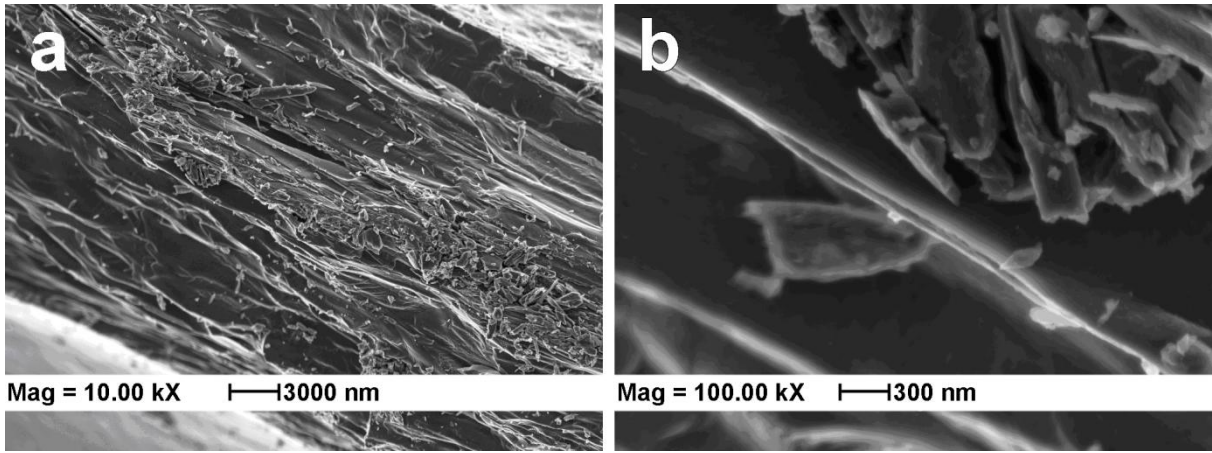


**Fig. 16.** SEM micrographs of semicokes of Pitch A obtained at 700°C for 120 min showing a) turbostratic structures and b) expansion of layers.

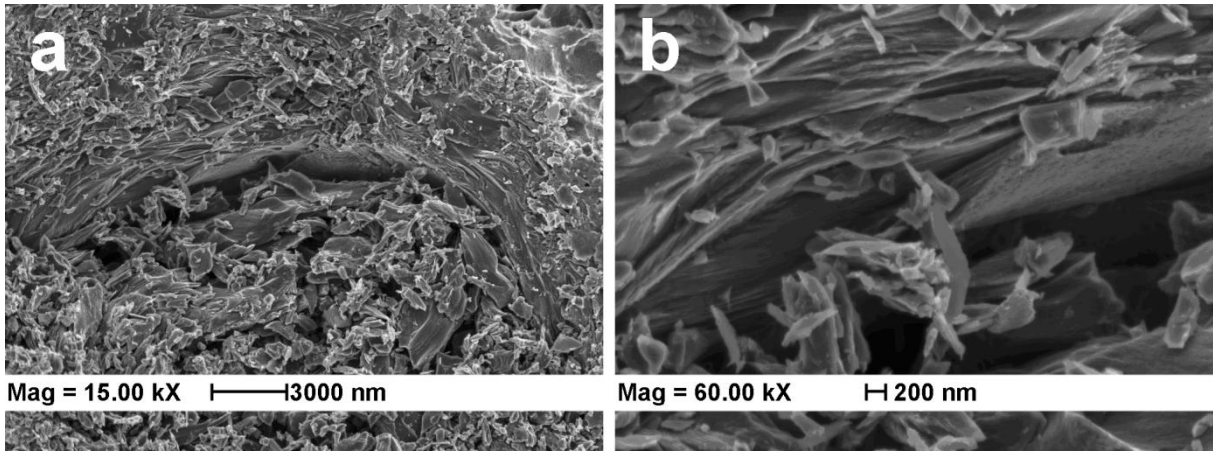


**Fig. 17.** SEM micrographs of semicokes of Pitch A obtained at 800°C for 120 min showing high turbostratic structure content at a) 15KX and b) 60KX magnifications.

**Table 1**

Elemental analysis data for Pitch A and Pitch B, wt %.

	N	C	H	S	H/C
Pitch A	0.7	82.9	9.7	6.5	1.40
Pitch B	0.6	85.2	10.2	4.0	1.44

1  
2  
3  
4  
5  
6  
7  
8  
9  
10  
11  
12  
13  
14  
15  
16  
17  
18  
19  
20  
21  
22  
23  
24  
25  
26  
27  
28  
29  
30  
31  
32  
33  
34  
35  
36  
37  
38  
39  
40  
41  
42  
43  
44  
45  
46  
47  
48  
49  
50  
51  
52  
53  
54  
55  
56  
57  
58  
59  
60  
61  
62  
63  
64  
65

**Table 2**

Percent areas of functional groups calculated from the deconvoluted  $^{13}\text{C}$  NMR spectra of the carbonaceous solid residues obtained from Pitch A and Pitch B.

Functional groups	Pitch A	Pitch B
	Area, %	Area, %
Ar-C=O	1.2	8.7
Ar-COOH	23.7	26.2
Ar-C	9.7	1.5
Ar-H	19.7	27.5
R-O-R	2.4	3.1
R-OH	13.2	14.9
-CH <sub>2</sub>	20.2	11.3
-CH <sub>3</sub>	9.8	6.6

**Table 3**  
Parameters of D Band.

Sample	Wavenumber (cm <sup>-1</sup> )	Height	Width	Area	Absolute Intensity	I <sub>D</sub> /I <sub>G</sub>
Pitch A 500°C 2h	1354	1321	86	5.6 x 10 <sup>6</sup>	6677	0.7
Pitch A 700°C 2h	1360	822	108	1.3 x 10 <sup>6</sup>	2389	0.8
Pitch A 900°C 2h	1332	60	3	2.2 x 10 <sup>5</sup>	610	0.9
Pitch A 900°C 1h	1408	71	4	2.3 x 10 <sup>4</sup>	409	0.9
Pitch A 900°C 30 min	1344	355	47	2.5 x 10 <sup>5</sup>	669	1.0
Pitch A 500°C 1h	1352	1636	105	3.5 x 10 <sup>6</sup>	5272	0.6
Pitch A 500°C 30 min	1354	822	64	3.4 x 10 <sup>6</sup>	4534	0.7
Pitch B 500°C 2h	1354	1954	103	5.6 x 10 <sup>6</sup>	7129	0.6
Pitch B 700°C 2h	1342	662	106	7.6 x 10 <sup>5</sup>	1556	0.7
Pitch B 1000°C 2h	1366	72	4	9.0 x 10 <sup>4</sup>	336	1.0

**Table 4**  
Parameters of G Band.

Sample	Wavenumber	Height	Width	Area	Absolute Intensity
Pitch A 500°C 2h	1590	4980	66	3.1x10 <sup>6</sup>	10283
Pitch A 700°C 2h	1597	1635	83	8.8 x 10 <sup>5</sup>	3028
Pitch A 900°C 2h	1604	366	64	1.8 x 10 <sup>5</sup>	666
Pitch A 900°C 1h	1600	97	7	8.1 x 10 <sup>4</sup>	484
Pitch A 900°C 30 min	1600	424	78	1.7 x 10 <sup>5</sup>	704
Pitch A 500°C 1h	1593	4619	64	2.3 x 10 <sup>6</sup>	8298
Pitch A 500°C 30 min	1591	2248	67	1.9 x 10 <sup>6</sup>	5759
Pitch B 500°C 2h	1597	5331	58	3.0 x 10 <sup>6</sup>	11252
Pitch B 700°C 2h	1592	1429	70	5.0 x 10 <sup>5</sup>	2242
Pitch B 1000°C 2h	1595	46	5	5.7 x 10 <sup>4</sup>	354

**Table 5**

Interlayer distances,  $d_{002}$ , of Pitch A and Pitch B semicokes with respect to temperature and pyrolysis time.

	$d_{002}$ , nm ( $d_{002, \text{graphite}} = 0.334$ nm)					
<b>Pitch A</b>	500°C	600°C	700°C	800°C	900°C	1000°C
30 min	0.350	0.352	0.350	0.349	0.354	0.356
60 min	0.353	0.353	0.349	0.351	0.353	0.354
120 min	0.351	0.352	0.347	0.352	0.350	0.346
<b>Pitch B</b>						
30 min	0.351	0.354	0.356	0.346	0.358	0.347
60 min	0.352	0.355	0.362	0.351	0.350	0.356
120 min	0.347	0.351	0.349	0.349	0.357	0.353

**Table 1**

Elemental analysis data for Pitch A and Pitch B, wt %.

	N	C	H	S	H/C
Pitch A	0.7	82.9	9.7	6.5	1.40
Pitch B	0.6	85.2	10.2	4.0	1.44

**Table 2**

Percent areas of functional groups calculated from the deconvoluted  $^{13}\text{C}$  NMR spectra of the carbonaceous solid residues obtained from Pitch A and Pitch B.

Functional groups	Pitch A	Pitch B
	Area, %	Area, %
Ar-C=O	1.2	8.7
Ar-COOH	23.7	26.2
Ar-C	9.7	1.5
Ar-H	19.7	27.5
R-O-R	2.4	3.1
R-OH	13.2	14.9
-CH <sub>2</sub>	20.2	11.3
-CH <sub>3</sub>	9.8	6.6

**Table 3**

Parameters of D Band.

Sample	Wavenumber (cm <sup>-1</sup> )	Height	Width	Area	Absolute Intensity	I <sub>D</sub> /I <sub>G</sub>
Pitch A 500°C 2h	1354	1321	86	5.6 x 10 <sup>6</sup>	6677	0.7
Pitch A 700°C 2h	1360	822	108	1.3 x 10 <sup>6</sup>	2389	0.8
Pitch A 900°C 2h	1332	60	3	2.2 x 10 <sup>5</sup>	610	0.9
Pitch A 900°C 1h	1408	71	4	2.3 x 10 <sup>4</sup>	409	0.9
Pitch A 900°C 30 min	1344	355	47	2.5 x 10 <sup>5</sup>	669	1.0
Pitch A 500°C 1h	1352	1636	105	3.5 x 10 <sup>6</sup>	5272	0.6
Pitch A 500°C 30 min	1354	822	64	3.4 x 10 <sup>6</sup>	4534	0.7
Pitch B 500°C 2h	1354	1954	103	5.6 x 10 <sup>6</sup>	7129	0.6
Pitch B 700°C 2h	1342	662	106	7.6 x 10 <sup>5</sup>	1556	0.7
Pitch B 1000°C 2h	1366	72	4	9.0 x 10 <sup>4</sup>	336	1.0

**Table 4**

Parameters of G Band.

Sample	Wavenumber	Height	Width	Area	Absolute Intensity
Pitch A 500°C 2h	1590	4980	66	$3.1 \times 10^6$	10283
Pitch A 700°C 2h	1597	1635	83	$8.8 \times 10^5$	3028
Pitch A 900°C 2h	1604	366	64	$1.8 \times 10^5$	666
Pitch A 900°C 1h	1600	97	7	$8.1 \times 10^4$	484
Pitch A 900°C 30 min	1600	424	78	$1.7 \times 10^5$	704
Pitch A 500°C 1h	1593	4619	64	$2.3 \times 10^6$	8298
Pitch A 500°C 30 min	1591	2248	67	$1.9 \times 10^6$	5759
Pitch B 500°C 2h	1597	5331	58	$3.0 \times 10^6$	11252
Pitch B 700°C 2h	1592	1429	70	$5.0 \times 10^5$	2242
Pitch B 1000°C 2h	1595	46	5	$5.7 \times 10^4$	354

**Table 5**

Interlayer distances,  $d_{002}$ , of Pitch A and Pitch B semicokes with respect to temperature and pyrolysis time.

	$d_{002}$ , nm ( $d_{002, \text{graphite}} = 0.334$ nm)					
<b>Pitch A</b>	500°C	600°C	700°C	800°C	900°C	1000°C
30 min	0.350	0.352	0.350	0.349	0.354	0.356
60 min	0.353	0.353	0.349	0.351	0.353	0.354
120 min	0.351	0.352	0.347	0.352	0.350	0.346
<b>Pitch B</b>						
30 min	0.351	0.354	0.356	0.346	0.358	0.347
60 min	0.352	0.355	0.362	0.351	0.350	0.356
120 min	0.347	0.351	0.349	0.349	0.357	0.353

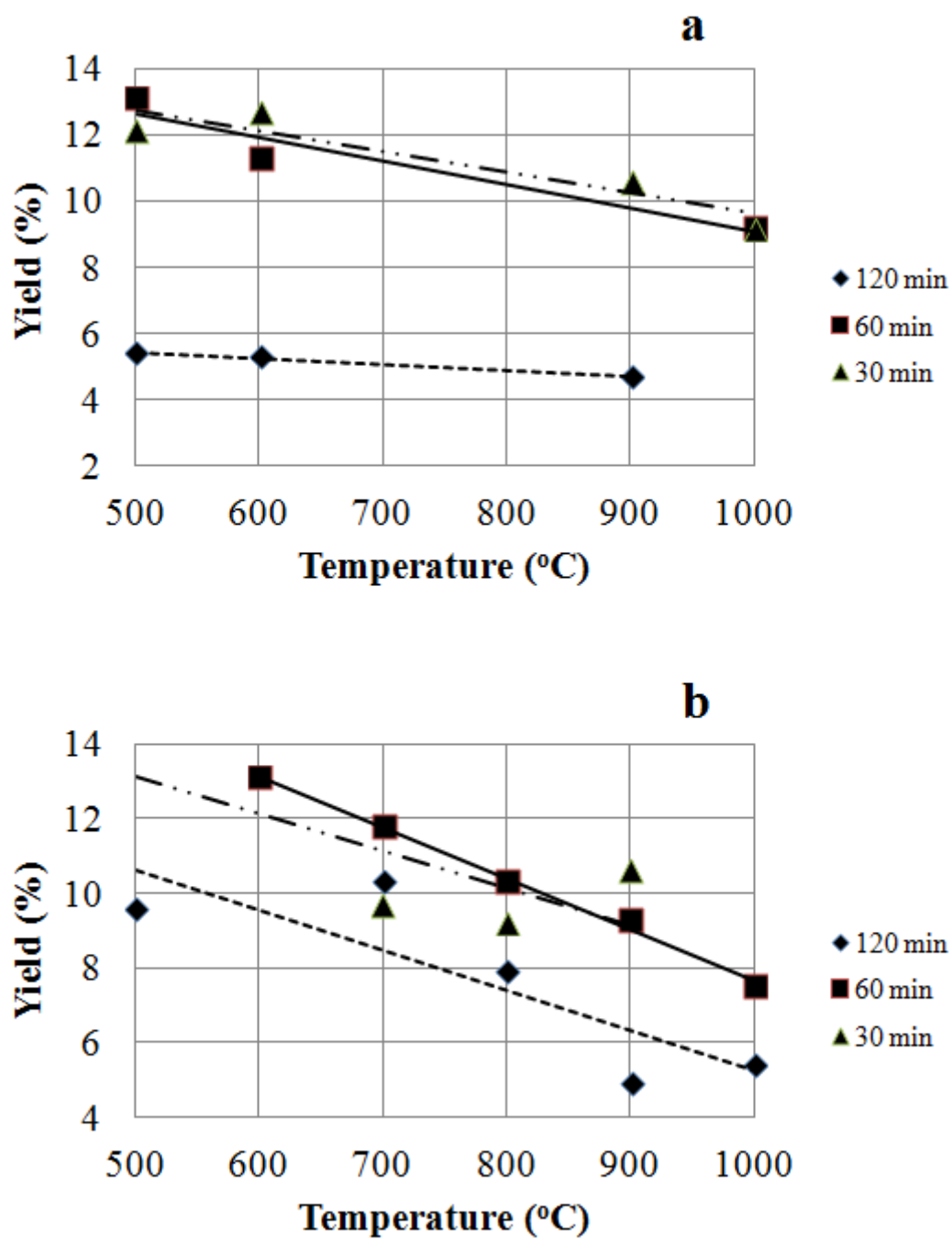


**Fig. 1.** Yields of semicokes of a) Pitch A and b) Pitch B with respect to pyrolysis temperature and time.

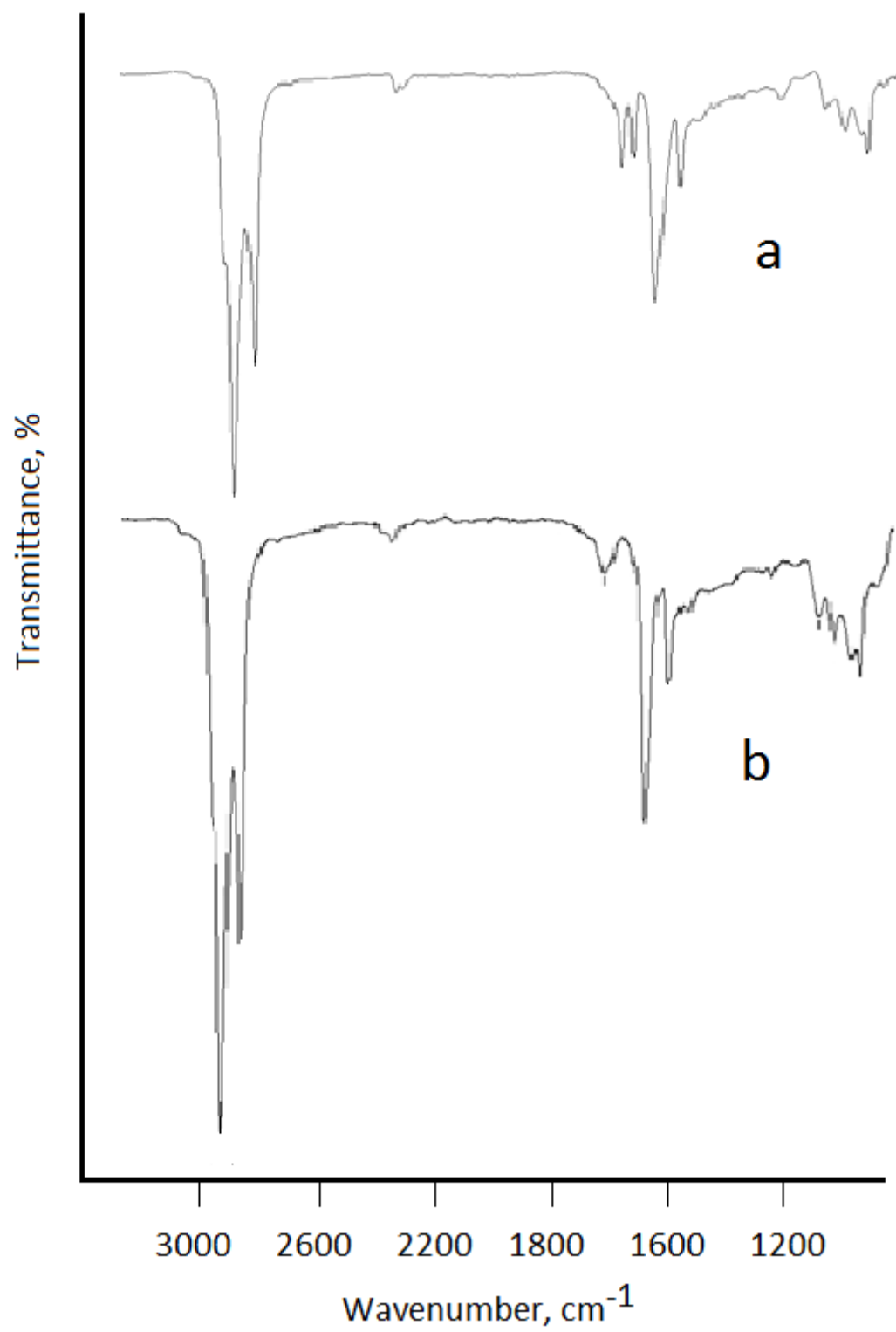


**Fig. 2.** FTIR spectra of a) Pitch A and b) Pitch B.

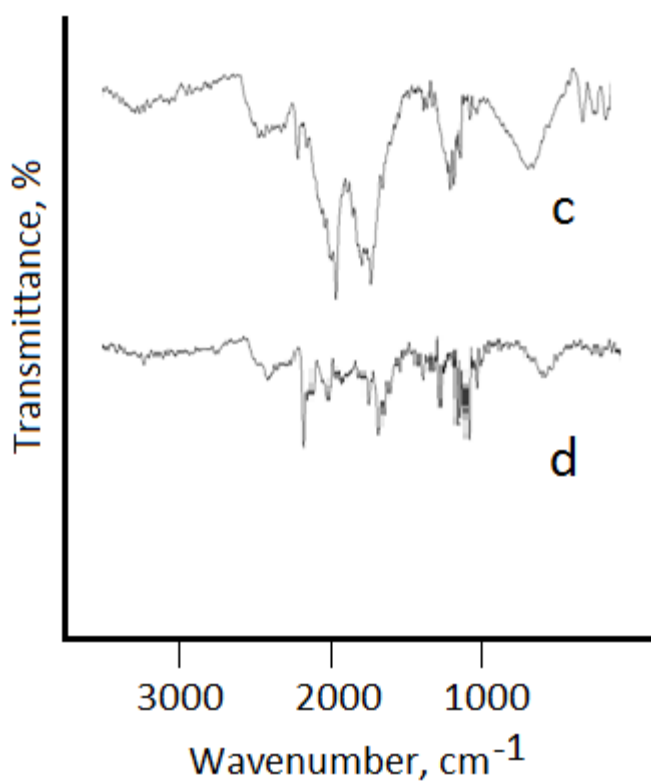
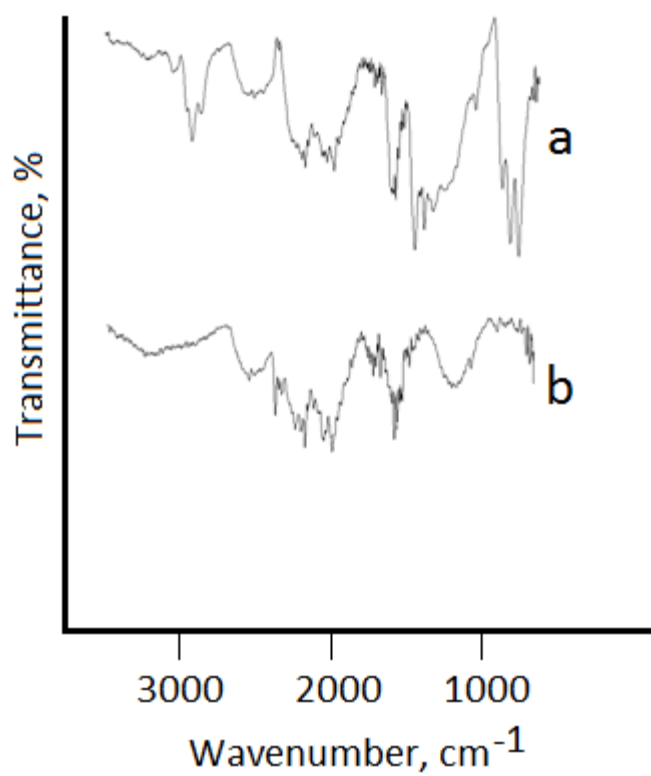


**Fig. 3.** FTIR spectra of semicokes obtained from pyrolysis of Pitch A after 120 min at a) 500°C, b) 900°C and from pyrolysis of Pitch B after 2h at c) 600°C, d) 1000°C.

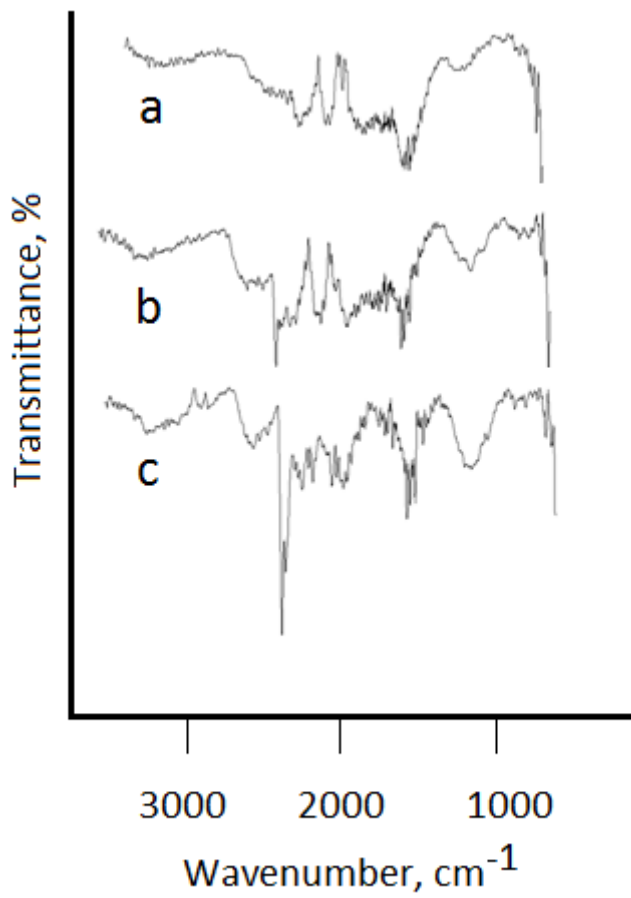


**Fig. 4.** FTIR spectra of semicokes from pyrolysis of Pitch A at 800°C for a) 30 min, b) 60 min and c) 120 min.

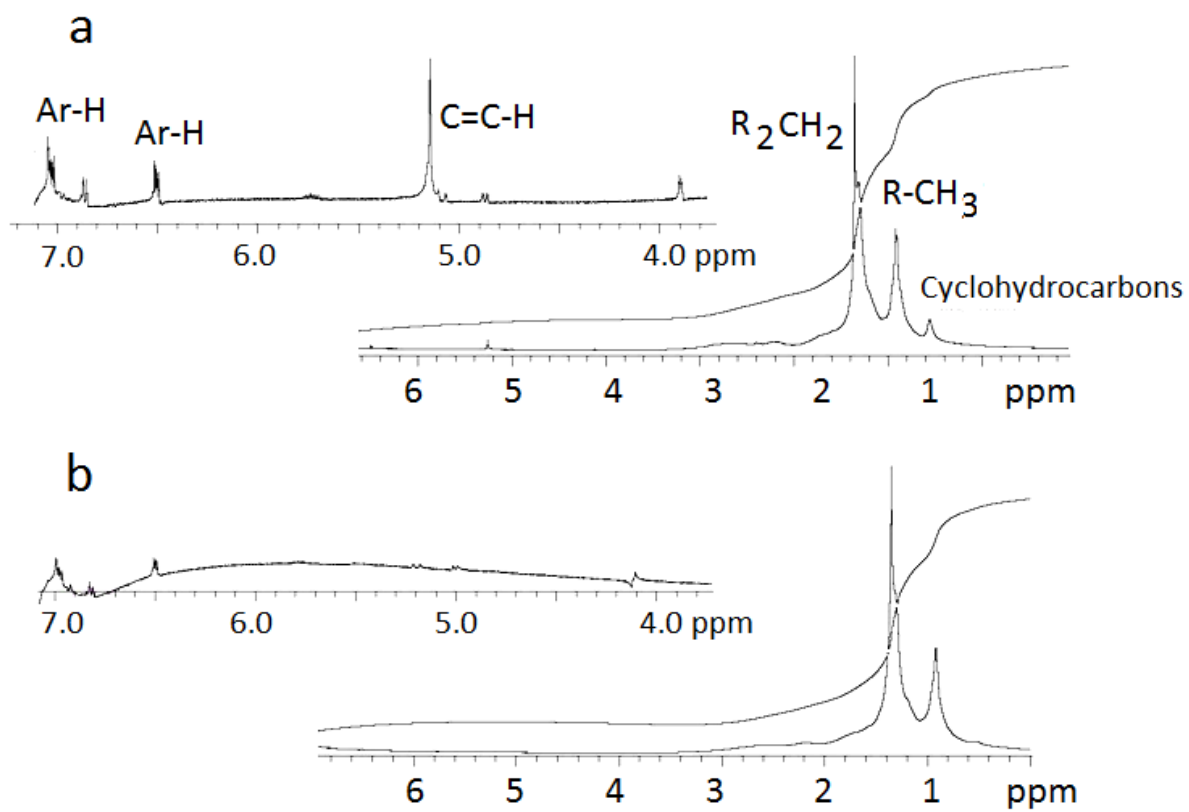


**Fig. 5.**  $^1\text{H-NMR}$  spectra of a) Pitch A and b) Pitch B.

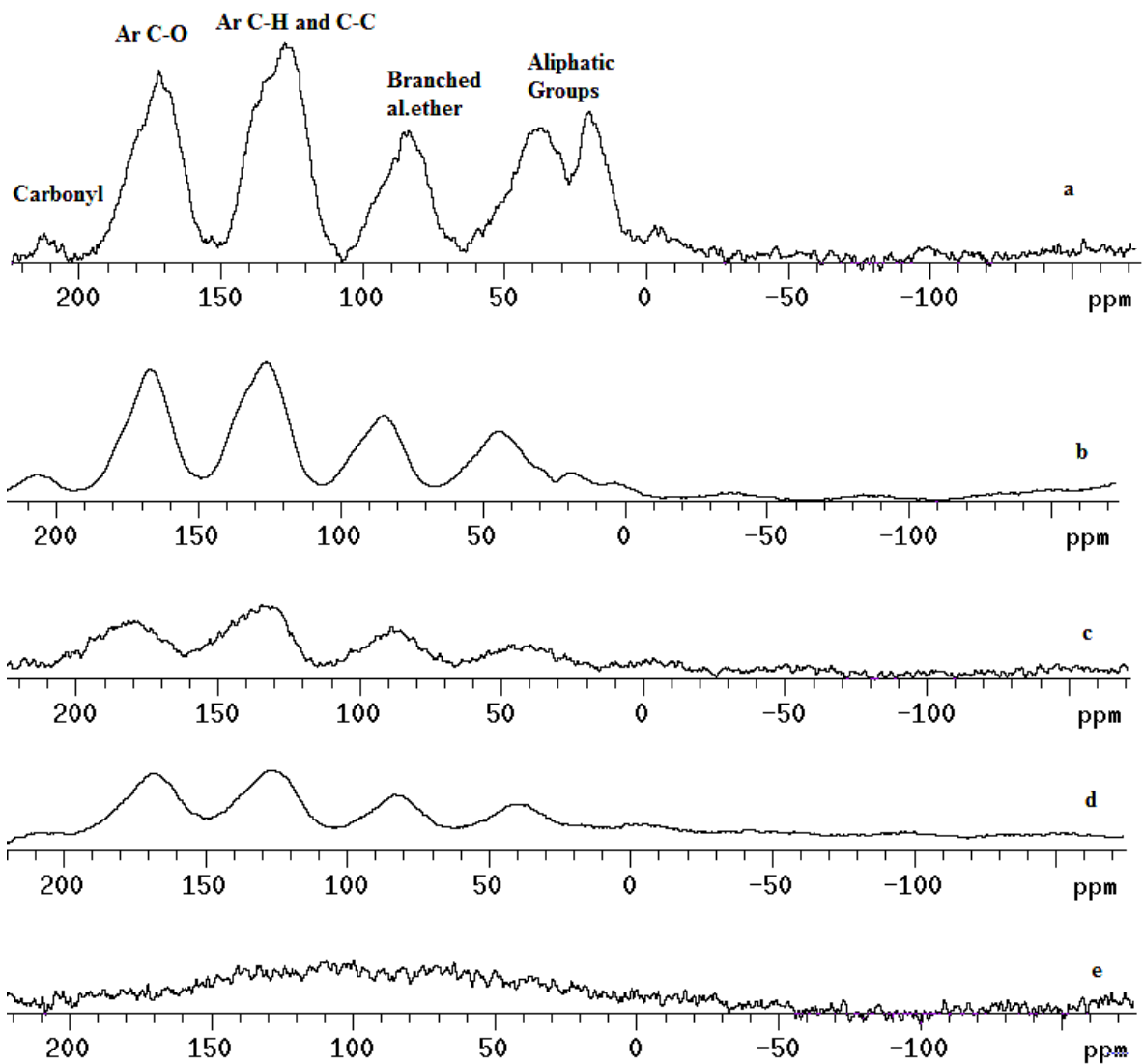


**Fig. 6.** Solid-state  $^{13}\text{C}$ -NMR spectra of semicokes of Pitch A for 120 min at a) 500°C, b) 600°C, c) 700°C, d) 800°C, and e) 900°C.

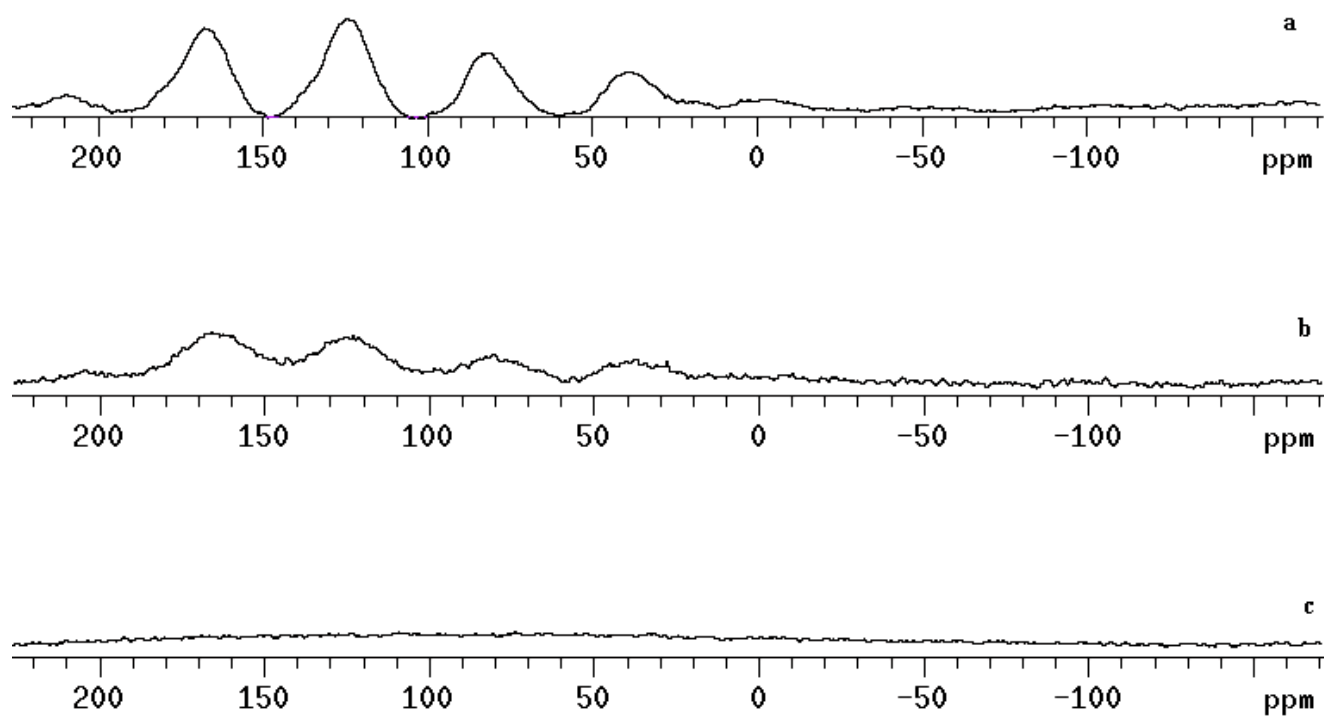


**Fig. 7.** Solid-state  $^{13}\text{C}$ -NMR spectra of semicokes of Pitch B for 120 min at a) 600°C, b) 800°C, and c) 1000°C.

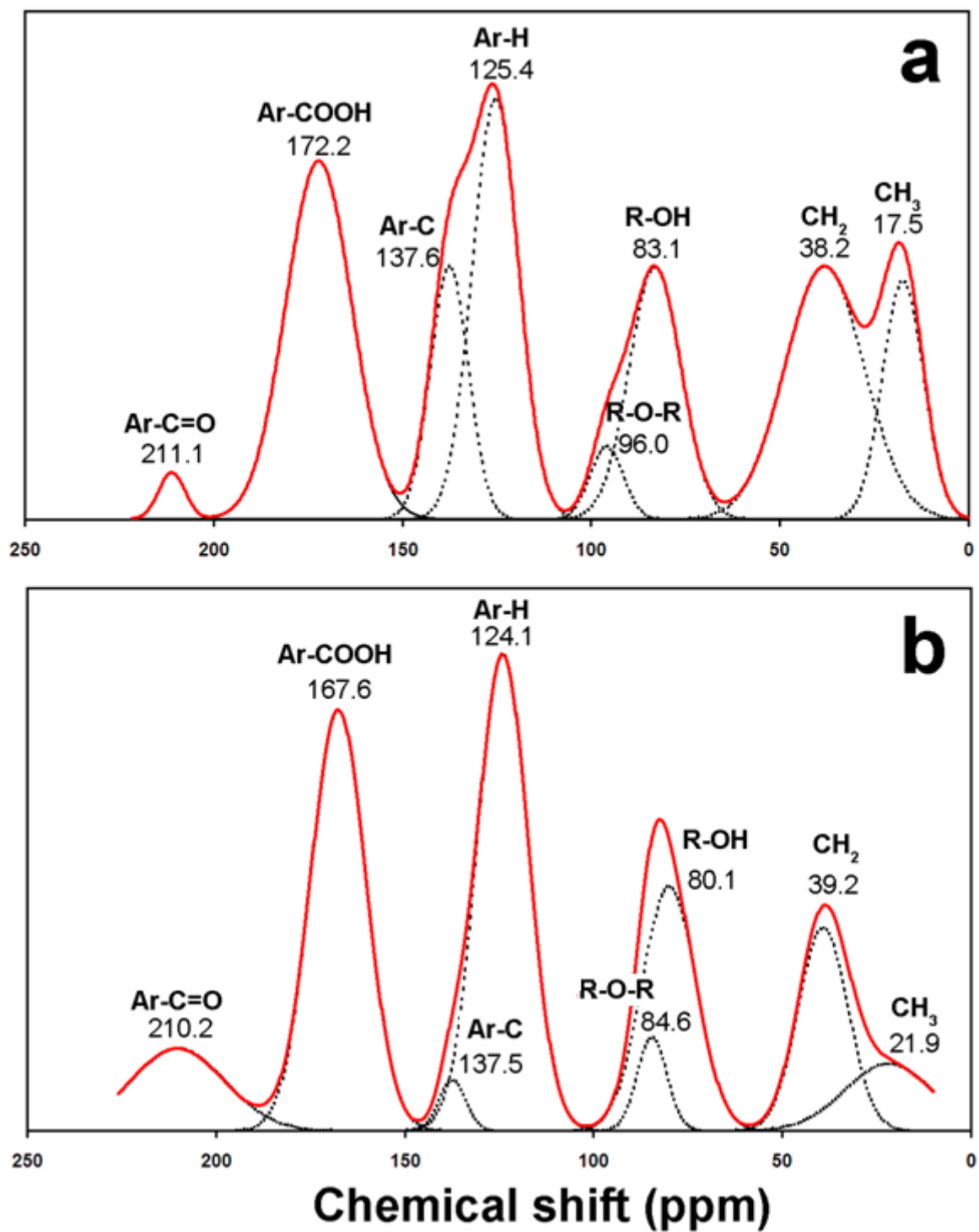


**Fig. 8.** Deconvoluted solid state  $^{13}\text{C}$  NMR spectra of semicokes from pyrolysis of a) Pitch A at  $500^\circ\text{C}$  for 120 min, b) Pitch B at  $600^\circ\text{C}$  for 120 min.

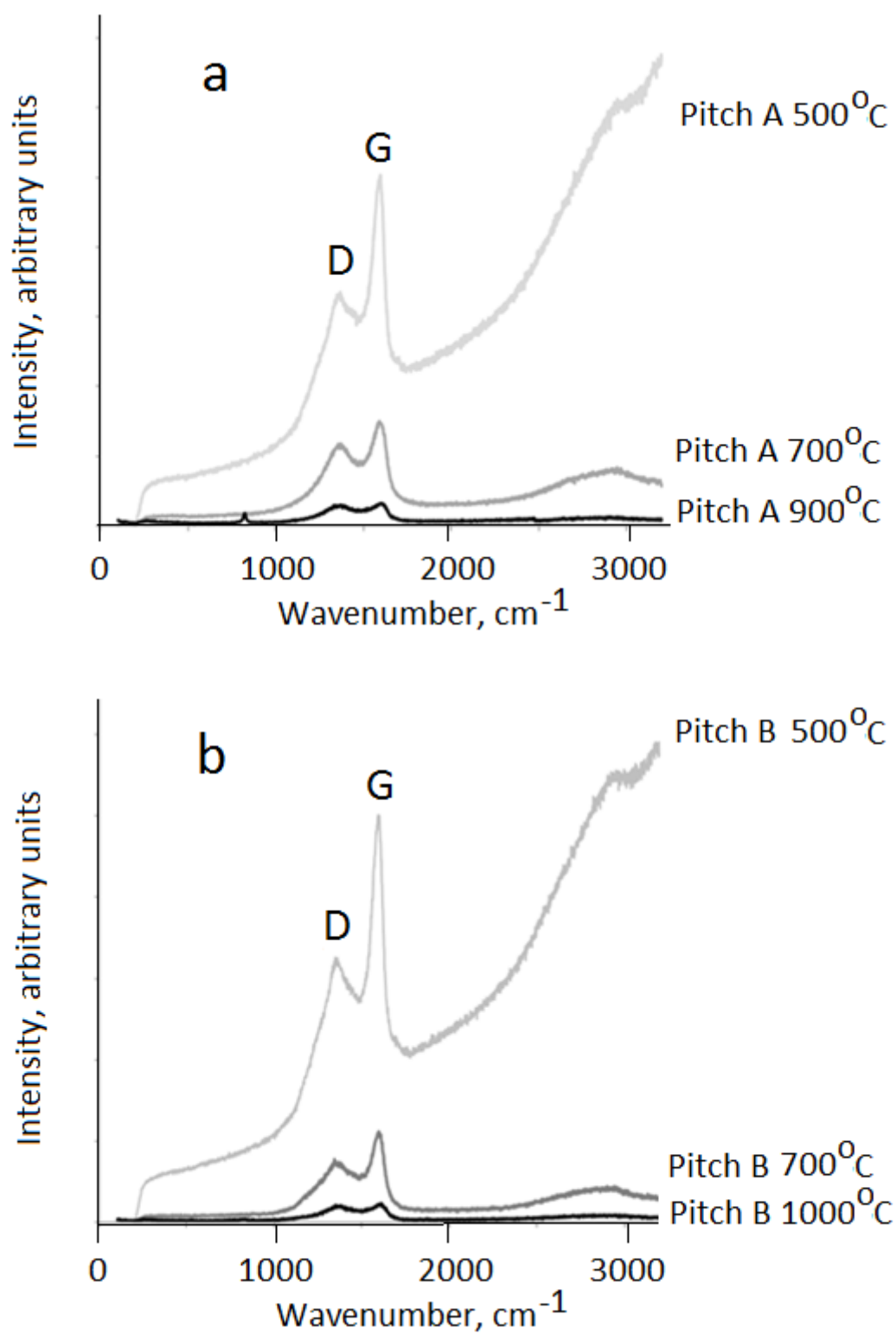


**Fig. 9.** Raman spectra of semicokes of a) Pitch A for 120 min at 500, 700 and 900°C and b) Pitch B for 120 min at 500, 700 and 1000°C.

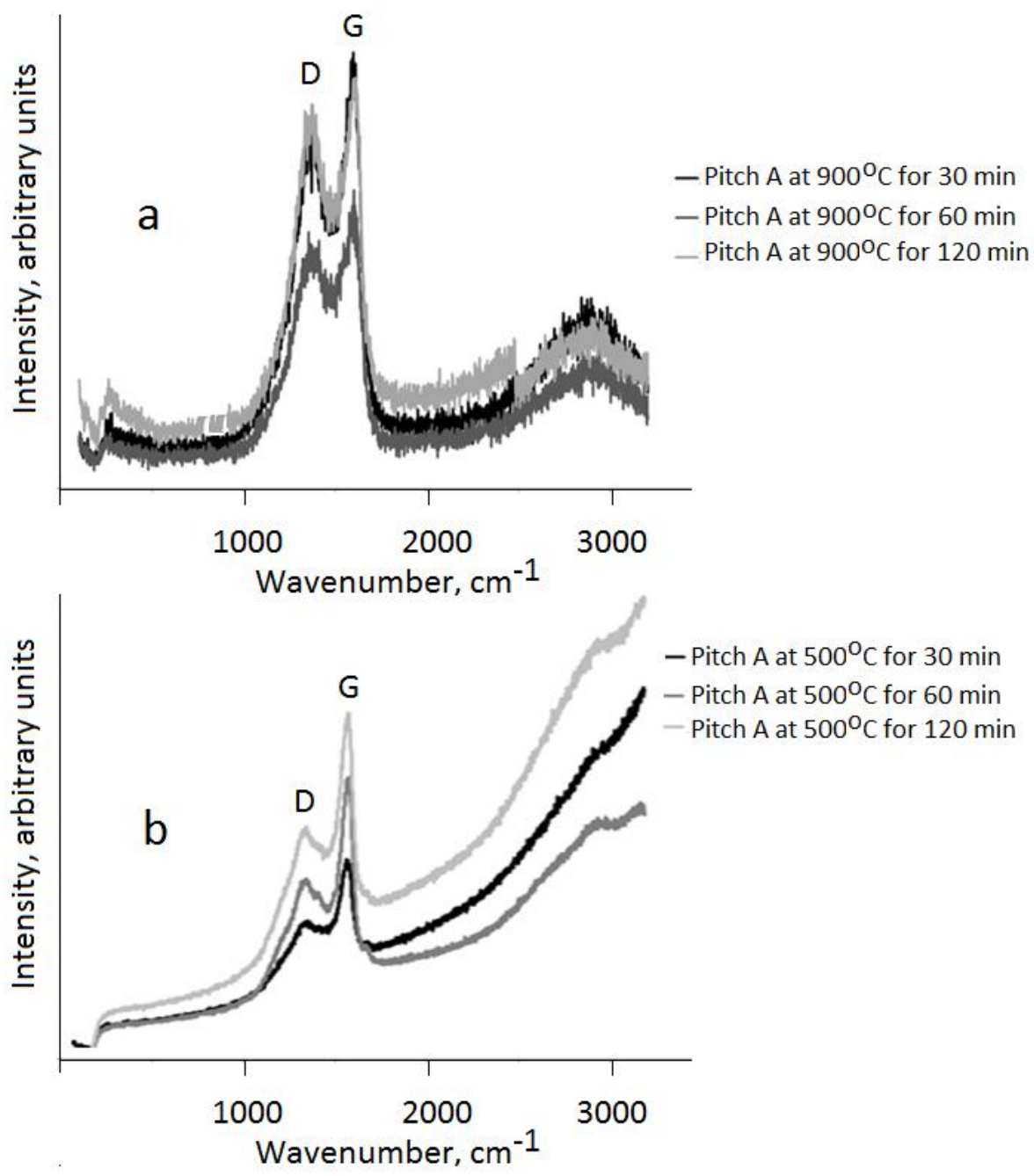


**Fig. 10.** Raman spectra of semicokes of Pitch A at a) 900°C and b) 500°C for 30, 60 and 120 min.

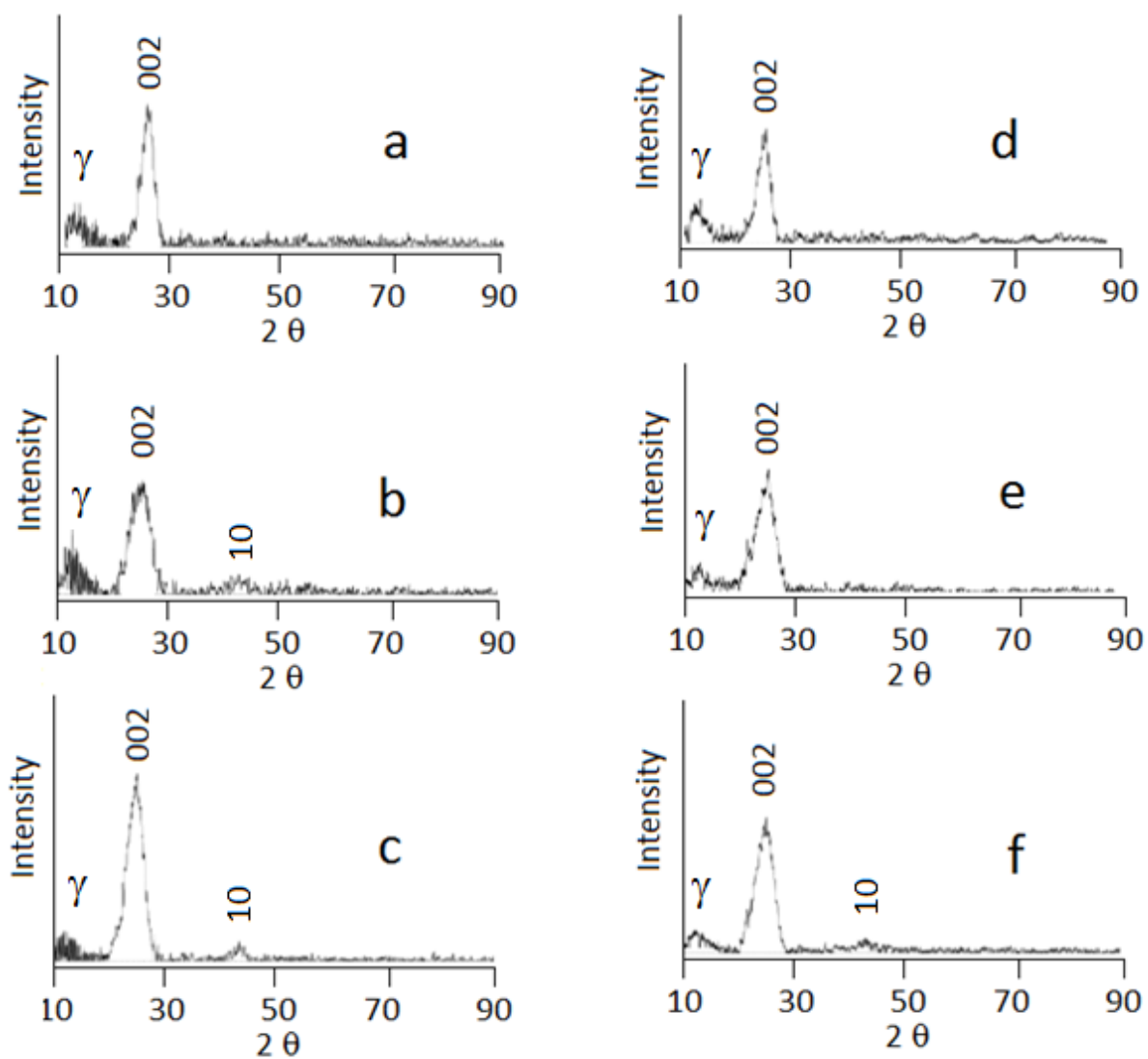


**Fig. 11.** X-ray diffraction pattern of semicokes produced from Pitch A pyrolysis for 120 min at a) 500°C, b) 700°C, and c) 1000°C, and from from Pitch B pyrolysis for 120 min at d) 500°C, e) 700°C, and f) 1000°C.

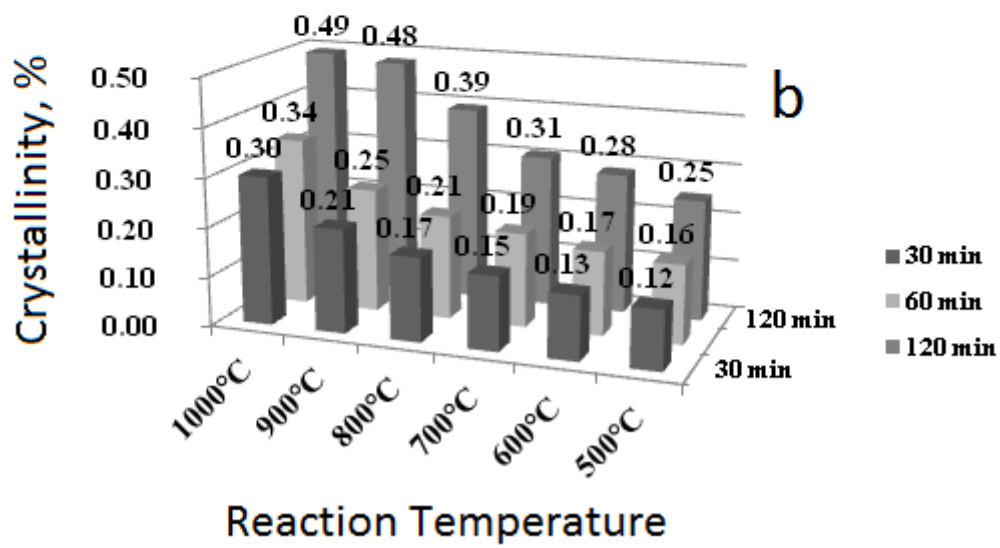
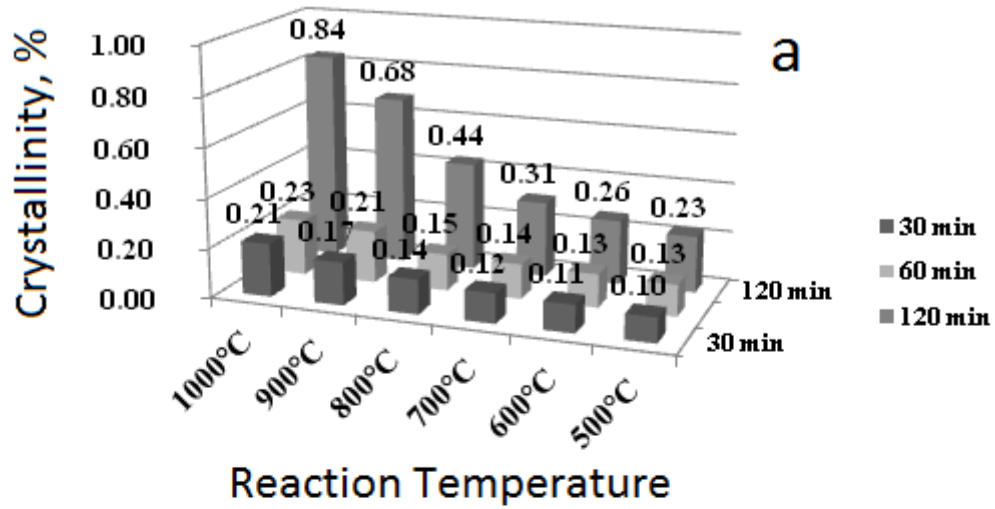


**Fig. 12.** Crystallinity of semicokes from pyrolysis of a) Pitch A and b) Pitch B.

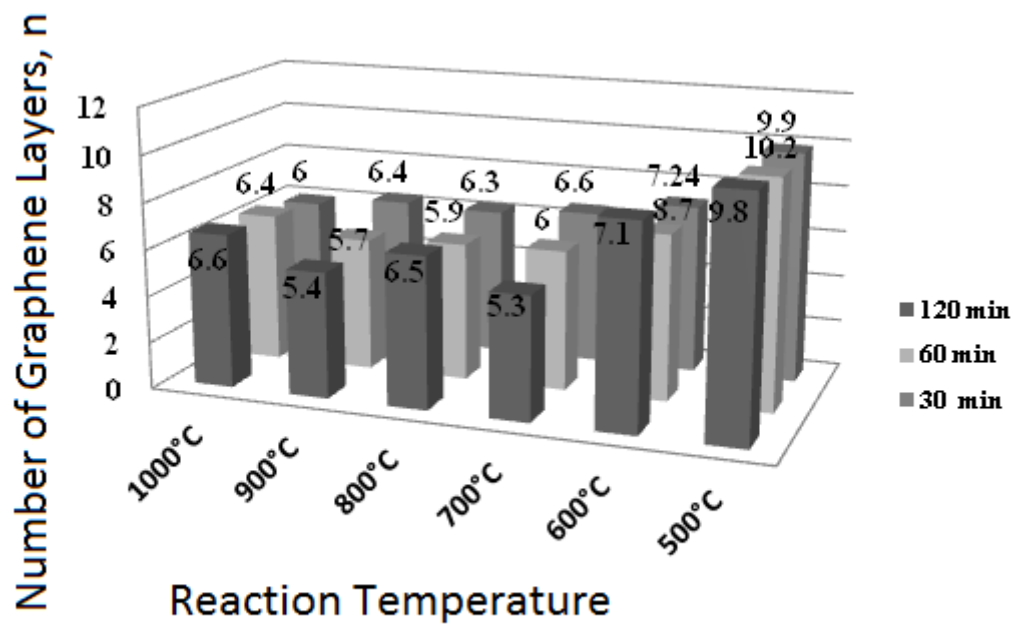


**Fig. 13.** Calculated  $n$  values of semicokes of Pitch A with respect to time and temperature.

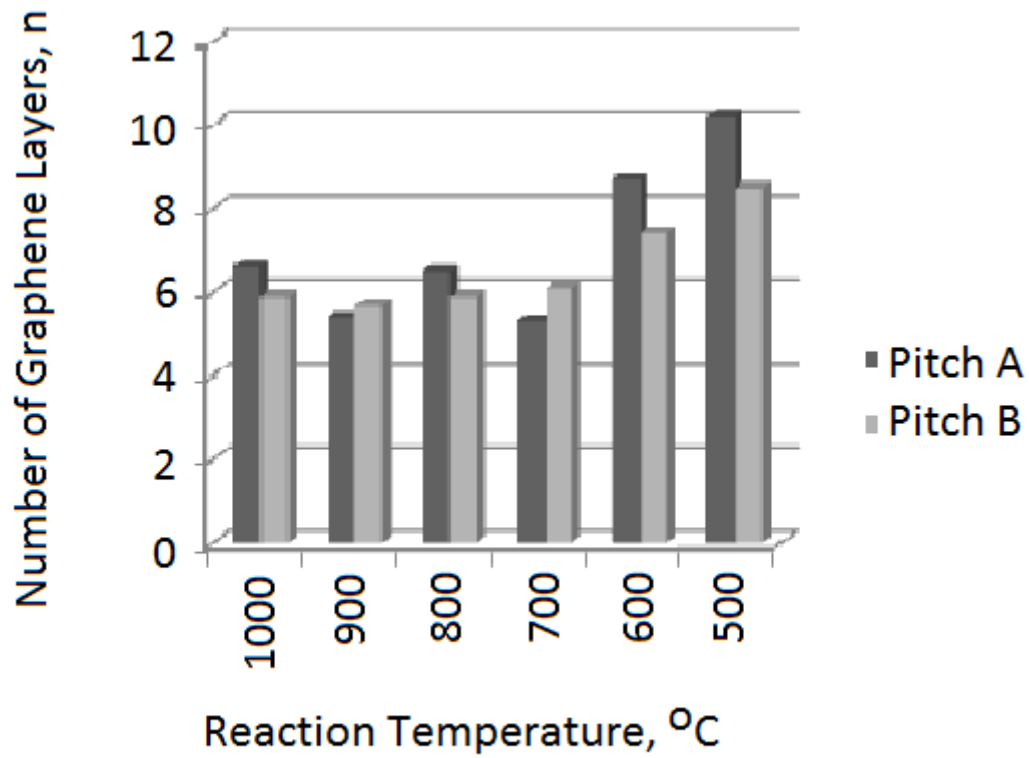


**Fig. 14.** Change in calculated  $n$  values of semicokes at 120 min pyrolysis with respect to pitch type and pyrolysis temperature.

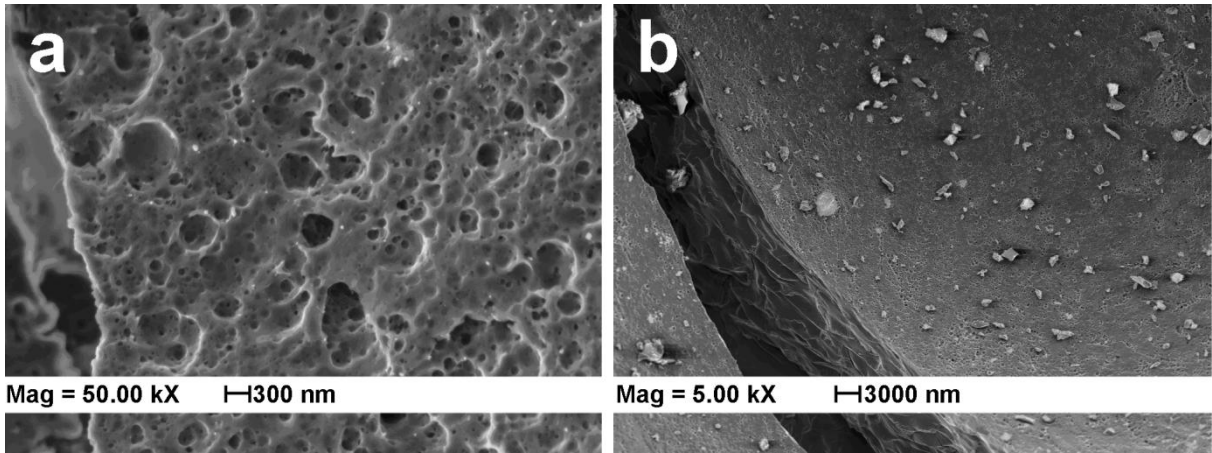


**Fig. 15.** SEM micrographs of semicokes of Pitch A obtained at 600°C for 120 min showing a) pores and b) layering structures.

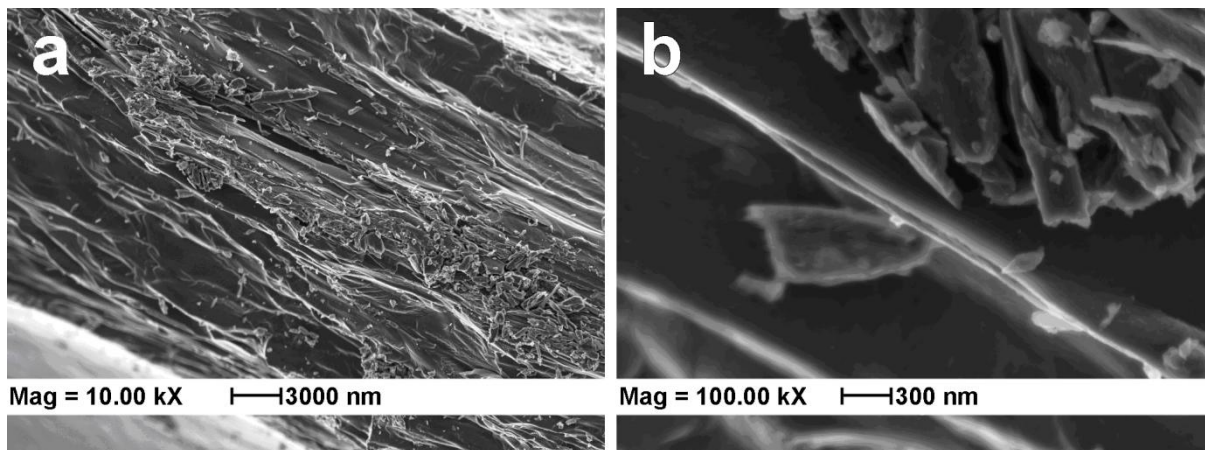


**Fig. 16.** SEM micrographs of semicokes of Pitch A obtained at 700°C for 120 min showing a) turbostratic structures and b) expansion of layers.

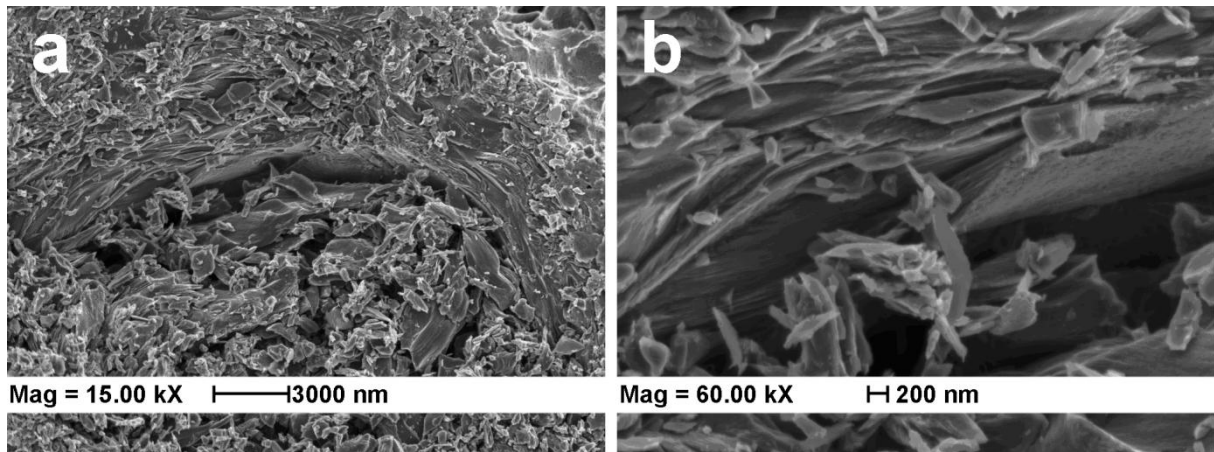


**Fig. 17.** SEM micrographs of semicokes of Pitch A obtained at 800°C for 120 min showing high turbostratic structure content at a) 15KX and b) 60KX magnifications.

## Highlights

- The present study focuses on the structural analysis of anisotropic semicokes of the pyrolysis of petroleum pitches obtained under various experimental conditions of temperature and time.
- Detailed information of factors which influence formation of anisotropy or turbostratic structures in resultant semicokes are given.
- FTIR,  $^1\text{H-NMR}$ , and  $^{13}\text{C-NMR}$  results showed that the aromatic structure of the semicokes was increasing with respect to increasing temperature as well as increasing time.
- XRD patterns of the semicokes showed the formation of some crystalline material with time and temperature.
- All the results of characterizations were consistent and indicated the formation of highly amorphous hydrocarbon materials that contain turbostratic structures.
- As the pyrolysis temperature was increased, aromatic structure formation was favored with increased crystallinity in the semicokes.